Polymer Degradation and Stability 250 (2026) 112212

Contents lists available at ScienceDirect

Polymer Degradation and Stability

journal homepage: www.journals.elsevier.com/polymer-degradation-and-stability

Mechanistic insights into the thermal decomposition of linear polyamidoamines via coupled TG–FTIR analysis

Jenny Alongi, Alessandro Beduini, Elisabetta Ranucci *

Dipartimento di Chimica, Università degli Studi di Milano, via C. Golgi 19, 20133, Milan, Italy

ARTICLE INFO

Keywords:
Linear polyamidoamines
Thermal decomposition
Thermo-oxidation
Cotton
Thermogravimetric-infrared analysis (TG-FTIR)

ABSTRACT

Linear polyamidoamines (PAAs), synthesized via the polyaddition of α-amino acids with N,N′-methylenebisacrylamide, act as effective intumescent flame retardants for cotton. Among the investigated systems, the glycine-derived PAA (M-GLY) achieved flame extinguishment in horizontal flame spread tests at add-on levels of 5–7%, whereas the arginine-derived analogue (M-ARG) required a significantly higher add-on (19%) to reach the same performance.

Thermogravimetric analysis (TGA) identified three main thermo-oxidative degradation stages, occurring in the ranges 50–250 °C, 250–400 °C, and 400–800 °C, corresponding to the onset of decomposition, completion of the primary mass-loss event, and the intumescence region, respectively. Hyphenated TGA–Fourier transform infrared spectroscopy (TG–FTIR), performed between 50 and 800 °C under both inert and oxidative atmospheres, enabled identification of the volatile species evolved within these temperature intervals. The results highlight subtle yet significant differences in the thermal decomposition pathways of the PAAs, enabling the proposal of a well-defined gas-phase protective mechanism during cotton combustion. The decomposition pathways involve an initial depolymerization step, followed by decarboxylation, deamination, and homolytic bond cleavage reactions, leading to the evolution of gaseous products that contribute to flame inhibition through dilution of oxygen and flame radicals. The thermal and thermo-oxidative decomposition of M-GLY and M-ARG was compared with those of M-MEP – deriving from N,N′-methylenebisacrylamide and 2-methylpiperazine, a non-self-extinguishing PAA adopted as a reference material. The proposed decomposition mechanism of M-MEP involves the extensive release of the volatile and combustible amine monomer 2-methylpiperazine, which accounts for its lack of protective effectiveness toward cotton during combustion.

1. Introduction

Linear polyamidoamines (PAAs) are multifunctional polymers obtained by the aza-Michael polyaddition of either primary or bis-secondary-amines with bis-acrylamides [1]. PAAs have attracted interest in various technical applications, for instance as bioactive polymers [2,3], resins for absorbing heavy-metal-ions for water purification [4], photostabilizers, [5] sensor coatings [6], and flame retardants (FRs) for cotton textiles [7].

Over the last decade, PAAs derived from N,N′-methylenebisacrylamide (MBA) and α-amino acids have emerged as efficient intumescent FRs for cotton. Consequently, significant effort has been devoted to elucidating their mode of action, which is a key prerequisite for the rational design of more effective and durable formulations [8,9]. The performance of these PAAs has been extensively assessed by horizontal (HFSTs) and vertical flame spread tests (VFSTs), enabling the identification of the minimum add-on levels required to achieve flame extinguishment [10,11]. Among the investigated systems, PAAs derived from glycine (M-GLY) and arginine (M-ARG) have drawn particular interest. Cotton treated with M-GLY self-extinguishes in HFSTs at add-ons ≥4–7%, while M-ARG is effective at add-ons ≥19%.

PAAs derived from α-amino acids swell and char upon direct flame exposure without igniting [10], and PAA-treated cotton forms carbonaceous chars above ca. 350 °C [10,11]. These chars are thought to exert a protective effect by limiting heat, oxygen and mass transfer between the flame and the underlying substrate. Morphological observations by scanning electron microscopy (SEM) and results from oxygen-consumption cone calorimetry further support this interpretation.

The intumescent behavior of PAAs is generally attributed to the

* Corresponding author.
E-mail address: elisabetta.ranucci@unimi.it (E. Ranucci).

https://doi.org/10.1016/j.polymdegradstab.2026.112212
Received 5 March 2026; Received in revised form 27 April 2026; Accepted 11 May 2026
Available online 12 May 2026

release of gaseous decomposition products, namely water, carbon dioxide, and ammonia, during thermal decomposition [7]. These gaseous species promote char expansion and concurrently dilute flame radicals and oxygen. Their generation arises from the thermally labile functional groups present in the PAA repeating units, particularly carboxyl and amine moieties. Importantly, PAAs undergo thermal decomposition within a temperature range that substantially overlaps with that of cotton [10,12], favoring an early interaction between the degradation pathways of the additive and the cellulosic substrate and thereby enhancing protective efficiency.

Previous investigations have primarily focused on the solid residues generated during the controlled thermo-oxidation of PAA-treated cotton. In particular, chars obtained from M-GLY-impregnated cotton at 300, 350 and 420 °C, corresponding to different stages of the charring process, have been extensively characterized by SEM, XPS, Raman spectroscopy and solid-state NMR [8]. These studies demonstrated that M-GLY promotes the formation of aromatic and nanographitic char structures at lower temperatures than untreated cotton, leading at 420 °C to more extended and condensed aromatic domains.

Complementary electron paramagnetic resonance (EPR) studies on chars from cotton impregnated with M-GLY, and M-CYSS and M-GLY_{50}—$CYSS_{50}$ – obtained from the polyaddition of MBA with cystine and a 1:1 cystine/glycine molar ratio – subjected to identical thermo-oxidative treatments revealed marked differences in radical concentration between bulk and surface layers, the latter being representative of more advanced oxidation stages [9]. These results highlighted a temperature-dependent protection efficiency and suggested that differences in aromatization degree and char porosity play a decisive role. Notably, the absence of surface radicals in samples treated at 350 °C indicated that the formation of a PAA-derived char layer effectively shields the cotton substrate from oxygen penetration.

Despite these advances, comparatively little attention has been paid to the volatile products evolved during thermo-oxidation of PAAs, which play a central role in intumescence, dilution of combustible gases and interaction with the degrading cellulose. In this context, hyphenated thermogravimetric analysis and infrared spectroscopy (TG–FTIR) represent powerful tools to correlate mass-loss events with the chemical nature and evolution of gaseous decomposition products in real time [13,14].

In the present study, TG–FTIR analysis is employed to investigate the thermal and thermo-oxidative decomposition of M-GLY and M-ARG, alongside M-MEP, obtained from the reaction of MBA with 2-methylpiperazine, which is intentionally selected as a reference system not derived from an α-amino acid and known to exhibit non-self-extinguishing behavior.

These polymers display markedly different responses under ignitability tests involving direct flame impingement on powders [10]. Specifically, M-GLY does not ignite; instead, its surface undergoes pyrolysis, forming a dark-brown, porous carbonaceous crust that effectively protects the underlying material, which remains largely unaltered, with minimal mass loss (<5%). M-ARG likewise resists ignition but undergoes partial volatilization, leaving off-white residues corresponding to approximately 45% of the initial mass. In contrast, M-MEP exhibits pronounced flammability, undergoing nearly complete combustion and volatilization (>90% mass loss).

Previous interpretations, grounded in the well-established tendency of β-aminoethylamides such as PAAs to undergo retro-Michael decomposition into acrylamides and amines upon heating [15], attributed these differences to the nature of the volatile species generated. In particular, the flammability of M-MEP was ascribed to the release of volatile and flammable 2-methylpiperazine (b.p. 155 °C), whereas the ignition resistance of M-GLY and M-ARG was linked to the formation of non-volatile amino acids, which can additionally promote carbon dioxide evolution. However, this mechanistic hypothesis has not yet been directly verified. The present work addresses this gap by providing a detailed, temperature-resolved analysis of the evolved gaseous species. By correlating mass-loss profiles with their infrared identification, TG–FTIR enabled direct insight into the decomposition pathways and the release of key species governing the intumescent behavior of these polyamidoamines.

2. Materials and methods

2.1. Materials

N,N'-methylenebisacrylamide (99%), glycine (> 99%), L-arginine (> 99%), 2-methylpiperazine (> 99%), D_2O (99.9%), DCl (35% in D_2O), fuming hydrochloric acid (HCl, ≥ 37% in water), lithium hydroxide monohydrate (LiOH · H_2O, ≥ 98%), were supplied by Sigma Aldrich (Milan, Italy).

2.2. Synthesis of PAAs

M-GLY: N,N′-methylenebisacrylamide (9.34 g, 60 mmol), glycine (4.55 g, 60 mmol) and lithium hydroxide monohydrate (2.58 g, 60 mmol) were suspended in distilled water (20 mL) and maintained under stirring at 50 °C until complete dissolution. The reacting solution was then left in the dark at 25 °C for five days. The resulting viscous solution was diluted, then acidified to pH 4.5 using 6 M aqueous HCl and finally freeze dried.

M-MEP was synthesized following the same procedure adopted for M-GLY. For the different reactivity of the arginine monomer, M-ARG solution was maintained at 45 °C for 10 days prior to dilution, acidification, and freeze drying.

The amounts of reagents used in the synthesis of PAAs are shown in Table 1.

2.3. Methods

Thermogravimetric analyses (TGA) were obtained from 50 to 800 °C in nitrogen and air using a Mettler-Toledo TGA/DSC 2 Star System instrument (Milan, Italy). PAAs (5 mg) were placed in alumina crucibles and heated with a 10 °C min^{-1} heating rate under a 50 mL min^{-1} nitrogen or air flow.

Thermogravimetric analyses coupled with infrared spectroscopy (TG-FTIR) were carried out using a Perkin Elmer TGA 4000 microbalance (Milan, Italy) interfaced to a Perkin-Elmer Frontier FT-IR/FIR spectrophotometer (Milan, Italy). PAAs (5 mg) were placed in alumina crucibles and heated with a 10 °C min^{-1} heating rate under a 100 mL min^{-1} gas flow. Spectra were recorded at intervals of 2.8 s in the 4000 - 500 cm^{-1} spectral range using a resolution of 4 cm^{-1}.

Molecular weights were assessed by Size Exclusion Chromatography (SEC). SEC traces were obtained with a Knauer Pump 1000 equipped with a Knauer Autosampler 3800, TSKgel G4000 PW and G3000 PW TosoHaas columns connected in series, Light Scattering (LS) Viscotek 270 Dual Detector, UV detector Waters model 486, operating at 230 nm,

Table 1
Reagent amounts for PAA synthesis and molecular weights of resulting samples [a].

Code	Amine monomer	Amount of amine (g)	LiOH · H_2O (g)	$\overline{M}_n$ [b]	PD [c]
M-GLY	glycine	4.55	2.58	7800	1.4
M-ARG	L-arginine	10.5	–	5900	1.5
M-MEP	2-methylpiperazine	6.07	–	8500	1.7

[a] All preparations were performed using 9.34 g MBA and 20 mL distilled water. [b] Number average molecular weight, determined by size exclusion chromatography. [c] Polydispersity.

and a refractive index detector Waters model 2410. The mobile phase was a 0.1 Tris buffer pH 8.10 ± 0.05. The flow rate was set at 1 mL min-1 and sample concentration was 20 mg mL^{-1}.

3. Results

3.1. Rationale of the study

The PAAs investigated in this study were synthesized following a previously reported procedure [10] (Scheme 1), by the aza-Michael polyaddition of N,N'-bisacrylamide with glycine (M-GLY), arginine (M-ARG) and 2-methylpiperazine (M-MEP). All polymers were fully soluble in water and in water–alcohol mixtures containing up to 50% alcohol. M-MEP also exhibited limited swelling in chloroform. Their structures were confirmed by ^{1}H NMR (Fig. 1) and FT-IR/ATR (Fig. S1 in Supplementary Material) spectroscopy, both showing good agreement with the expected molecular structures. The number-average molecular weights ($\overline{M}_n$), determined by size exclusion chromatography (SEC), were consistent with typical values reported for PAAs, with $\overline{M}_n$ values of 7800, 5900 and 8500 for M-GLY, M-ARG, and M-MEP, respectively (Table 1). Notably, based on our previous experience, no clear correlation has been observed between the molecular mass of PAAs and their flame retardant properties.

α-Amino acid-derived PAAs, including M-GLY and M-ARG, are amphoteric polymers with a pH-dependent charge distribution. The predominant ionic species at their working pH (pH 4.5) are shown in Fig. 2. For comparison, the same figure also reports the ionic species distribution of the PAA denoted M-MEP, which was selected as non-extinguishing reference PAA not derived from an α-amino acid.

The reported pH corresponds to the value typically employed under PAA combustion test conditions and reflects the pH at which these systems are conventionally stored, i.e., that of maximum stability. Based on our previous experience, the FR performance of PAAs does not exhibit a clear dependence on pH. Accordingly, deviations from this value have been considered only in cases of limited solubility under acidic conditions. The ionic species distribution (Fig. S2) of PAAs was determined from the pK_a values and following the method described in the Supplementary Material.

Understanding the thermo-oxidative decomposition mechanism of these PAAs is essential to clarify their influence on the thermo-oxidative decomposition of cotton and their role as flame retardants. Notably, PAAs thermally decompose over a temperature range that significantly overlaps with that of cotton (Fig. 3). This overlap promotes early-stage interactions between the decomposition pathways of the PAAs and the cellulosic substrate, thereby enhancing the overall protective efficiency.

To achieve this objective, the release of gaseous decomposition products from M-GLY, M-ARG and M-MEP during heating was investigated using the hyphenated TG–FTIR technique. The analyses were performed under both inert (nitrogen) and oxidative (air) atmospheres.

Fig. S3 reports the TGA curves and the corresponding 3D plots, whereas Figs. 4 and 5 report the TGA curves under nitrogen and air, respectively, across three selected temperature ranges (50–250 °C, 250–400 °C, and 400–800 °C). Representative 2D IR spectra of the gaseous decomposition products evolved within these temperature ranges are shown in Fig. 4 (nitrogen) and Fig. 5 (air).

The thermal behavior of the monomers, i.e. MBA, glycine (GLY), arginine (ARG) and 2-methylpiperazine (MEP), is presented in Figs. 6 and 7, and S4. Specifically, Fig. S4 reports the TGA curves and the corresponding 3D plots, whereas Figs. 6 and 7 present the TGA curves under nitrogen and air, respectively, across the three selected temperature ranges selected for PAAs. Representative 2D IR spectra of the gaseous decomposition products evolved within these temperature ranges are shown in Fig. 6 (nitrogen) and Fig. 7 (air).

Finally, the temperature-dependent evolution profiles of the main gaseous products released from PAAs and their respective monomers are compared under nitrogen (Figs. 8–10) and air (Figs. 11–13).

3.2. Thermogravimetric analysis of PAAs

The characteristic thermal data of M-GLY, M-ARG, and M-MEP, obtained from the TG-thermograms presented in Fig. 3, are shown in Table 2.

Notably, all PAAs show qualitatively comparable thermal decomposition behavior in both nitrogen and air. This similarity can reasonably be ascribed to their common backbone structure, comprising an MBA-derived unit linked to either a primary amine–derived (M-GLY and M-ARG) or secondary amine–derived (M-MEP) moiety.

To facilitate mechanistic interpretation, the investigated temperature range was systematically subdivided into three well-defined intervals, as discussed below. Table 3 summarizes the weight losses for

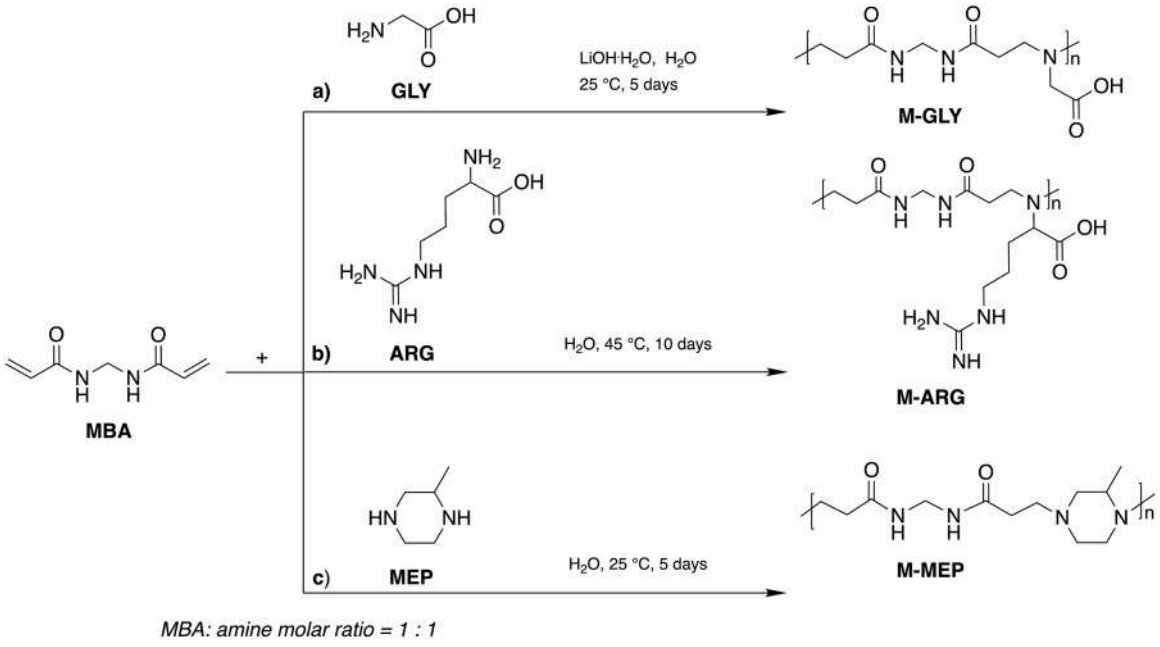

Scheme 1. Synthesis of PAAs.

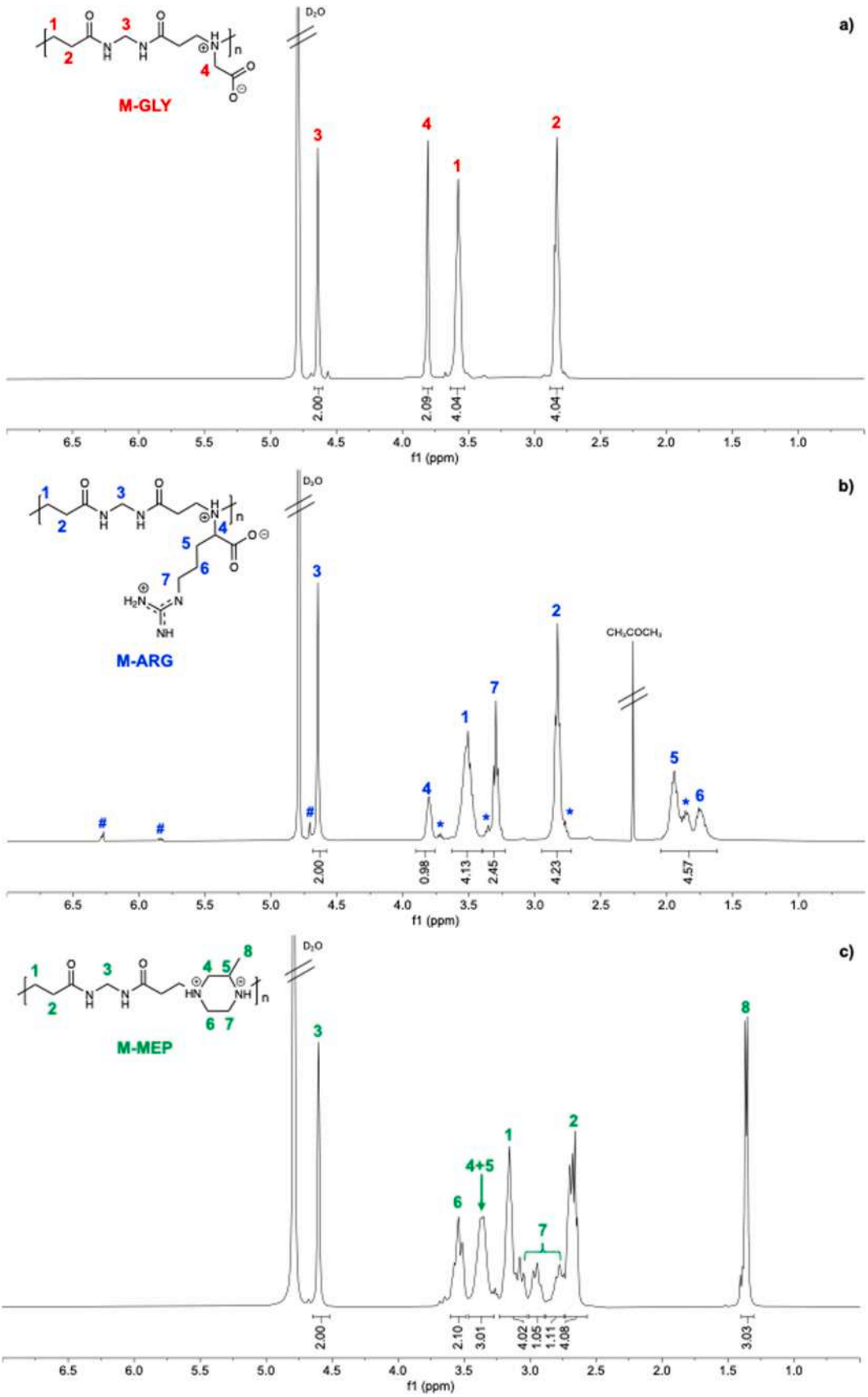

Fig. 1. ^{1}H NMR spectra in D_2O at pH 4.5 of M-GLY (a), M-ARG (b) and M-MEP (c).

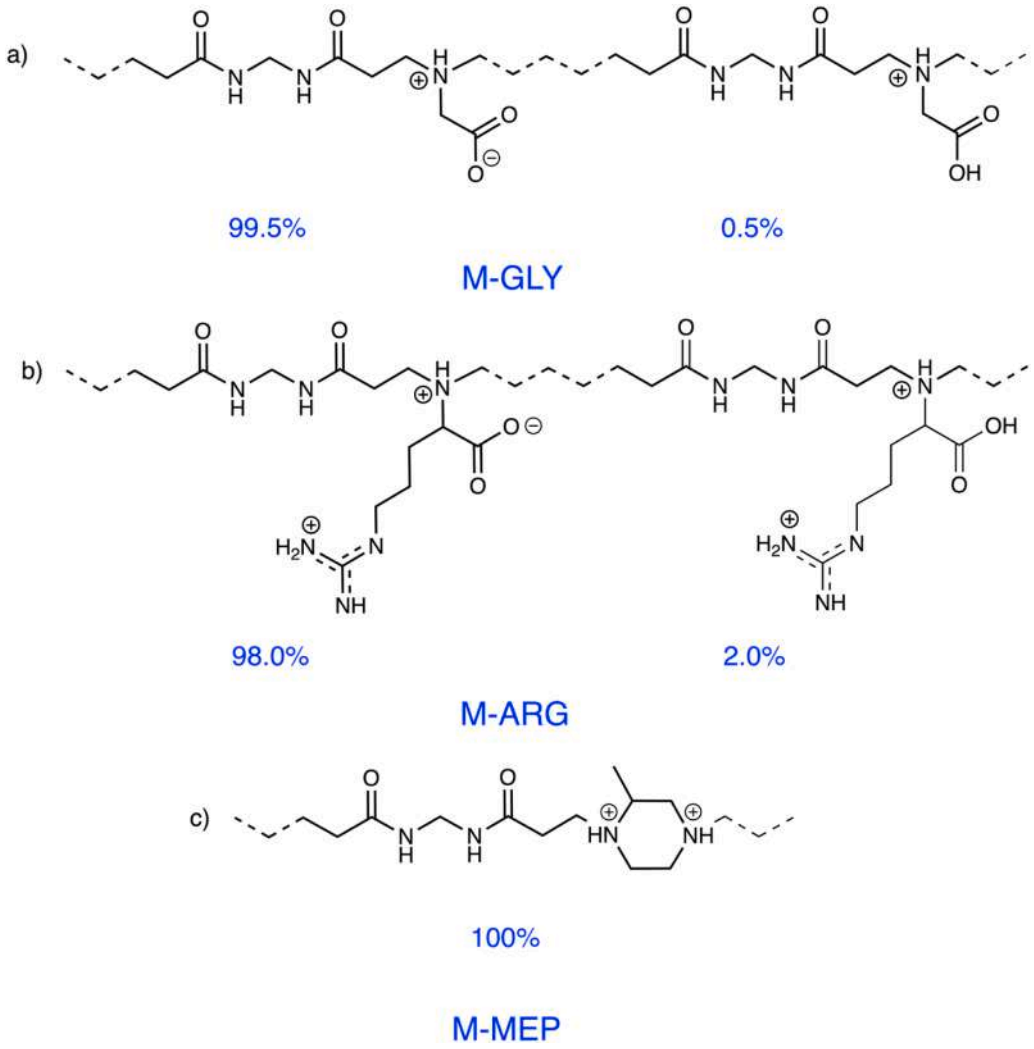

Fig. 2. Ionic species distribution at pH 4.5 for M-GLY (a), M-ARG (b) and M-MEP (c).

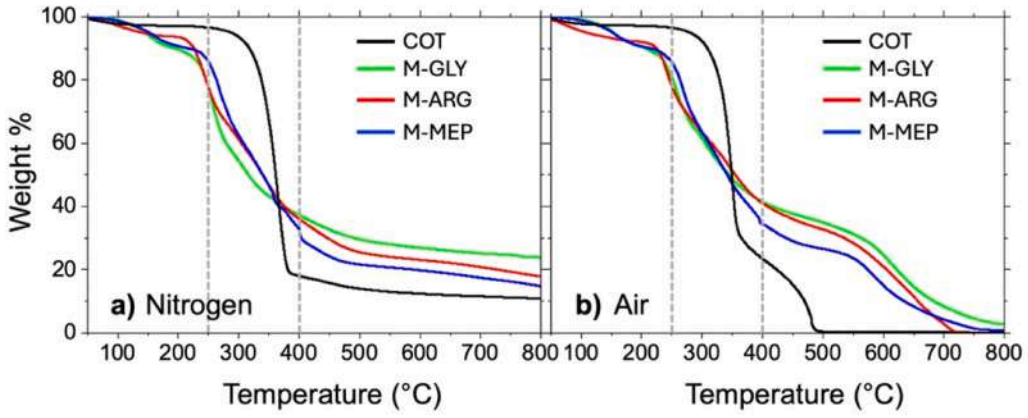

Fig. 3. TG-thermograms in inert (nitrogen, a) and oxidative (air, b) atmospheres of M-GLY, M-ARG, M-MEP and cotton.

these stages.

1st stage (50–250 °C). The thermograms obtained under nitrogen and air nearly overlap up to 250 °C (up to 450 °C in the case of M-GLY) (Fig. S3), showing the same $T_{onset10\%}$ (Table 2) and same weight loss in the temperature interval 50–250 °C (Table 3). This indicates that oxidative processes are kinetically insignificant within this temperature range, as previously reported for several polymeric systems [16]. Within this interval, all PAAs exhibit a mass loss of approximately 14–22%. This amount was almost completely achieved at approximately 150 °C, and mainly attributable to the evolution of water either loosely adsorbed or more strongly bound to the polymer backbone. The primary decomposition reactions that precede the major weight-loss occurring during the 2nd stage likely initiate between 150 and 250 °C.

2nd stage (250–400 °C). Within this temperature range, PAAs

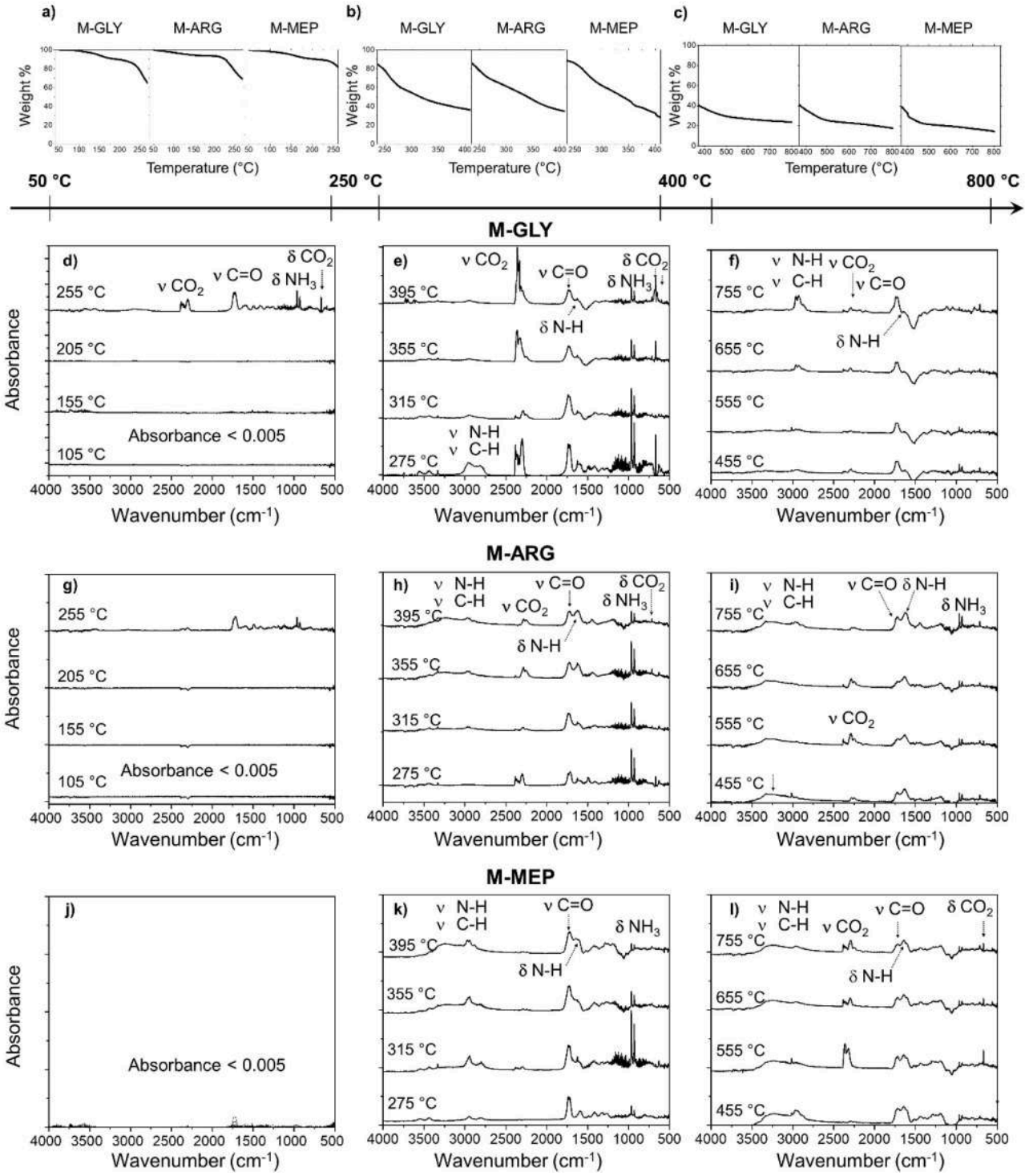

Fig. 4. TGA thermograms under inert atmosphere (N_2) of M-GLY, M-ARG and M-MEP in the temperature intervals 50–250 °C (a), 250–400 °C (b) and 400–800 °C (c). 2D plots of selected FT-IR spectra of the volatiles released under inert atmosphere (N_2) from M-GLY, M-ARG and M-MEP in the temperature intervals 50–250 °C (d,g,j), 250–400 °C (e,h,k) and 400–800 °C (f,i,l).

exhibit their most substantial mass loss, resulting from several concurrent decomposition processes, as commented below (Schemes 2–6). No significant differences were observed between the TG curves of M-MEP recorded under nitrogen and air atmospheres (Fig. S3). In contrast, for both M-GLY and M-ARG, the weight loss in air becomes less pronounced than that measured under nitrogen, albeit with some qualification. Specifically, the TG curves of both M-GLY and M-ARG obtained in nitrogen and air begin to diverge at approximately 250 °C (Fig. S3).

3rd stage (400–800 °C). Above 400 °C, oxidative reactions become kinetically significant and start to compete with purely pyrolytic pathways. In the 400–550 °C interval, the residual mass in air exceeds that measured under nitrogen, since oxidation contributes to the development and expansion of an intumescent char structure, promoting the formation of a swollen, protective carbonaceous layer [10]. At temperatures exceeding approximately 600 °C, however, oxidative char gasification becomes increasingly dominant, leading to its progressive

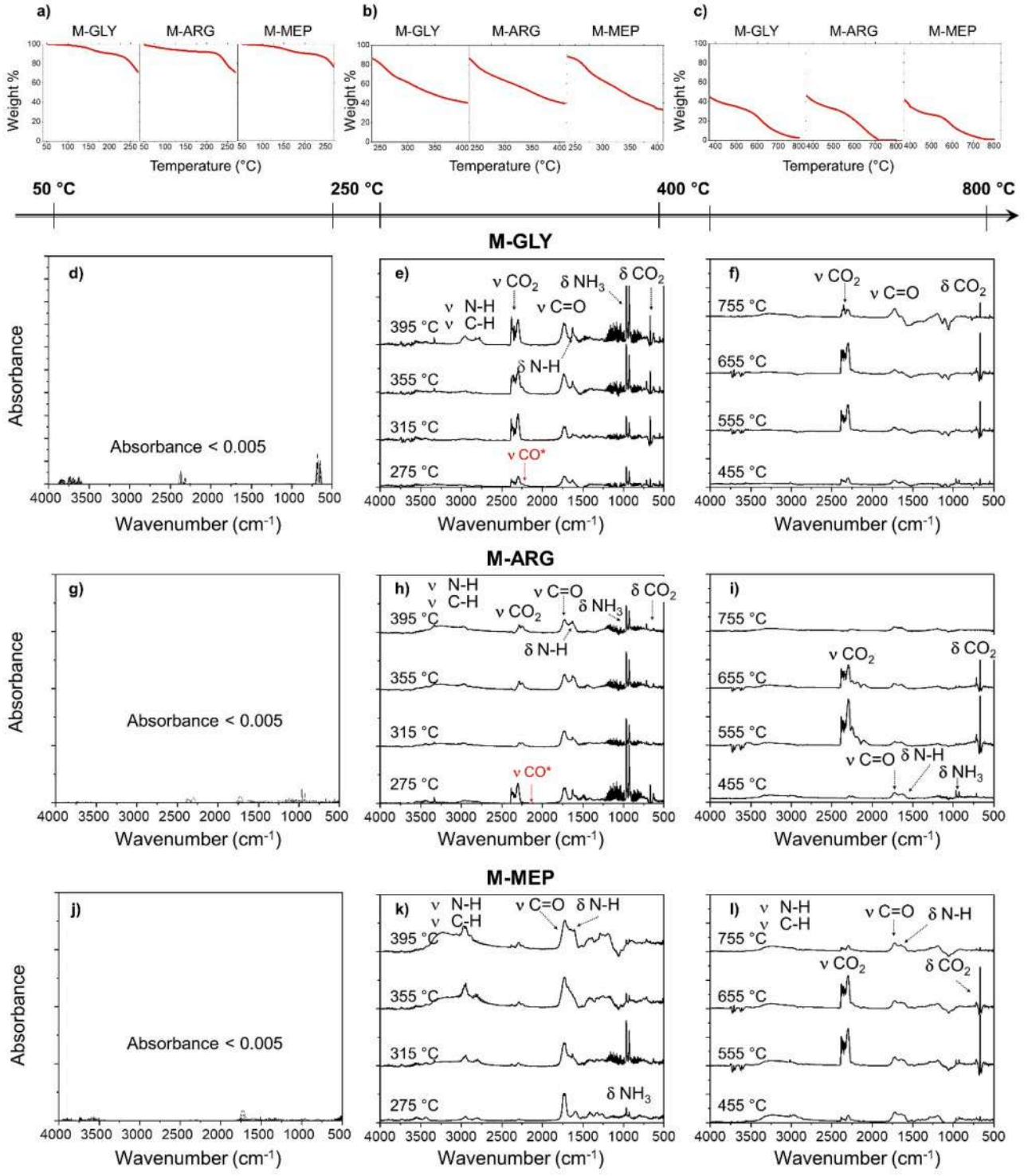

Fig. 5. TGA thermograms under oxidative atmosphere (air) of M-GLY, M-ARG and M-MEP in the temperature intervals 50–250 °C (a), 250–400 °C (b) and 400–800 °C (c). 2D plots of selected FT-IR spectra of the volatiles released under oxidative atmosphere (air) from M-GLY, M-ARG and M-MEP in the temperature intervals 50–250 °C (d,g,j), 250–400 °C (e,h,k) and 400–800 °C (f,i,l). *CO denotes that the concentration of carbon monoxide falls below the detection limit.

conversion into CO_2 and a consequent reduction in residual mass. Consequently, the TG traces recorded in air and nitrogen markedly diverge (Fig. S3).

Interestingly, M-GLY, M-ARG and M-MEP yielded significant char in nitrogen (23.8, 17.9 and 14.4%, respectively). M-GLY also yielded low but appreciable residue in air (2%), while M-ARG and M-MEP left minimal residues at 800 °C in air, suggesting predominant volatilization rather than stable char formation under oxidative conditions.

3.3. TG-FTIR analysis of PAAs

The composition of gases evolved during PAA thermal decomposition was determined by monitoring the characteristic IR absorption bands [17] of typical decomposition gases, including CO_2, CO, NH_3, and hydrocarbons (Table S1).

The 2D TG-FTIR analyses of the gaseous decomposition products of M-GLY, M-ARG and M-MEP between 50 and 800 °C reveal common

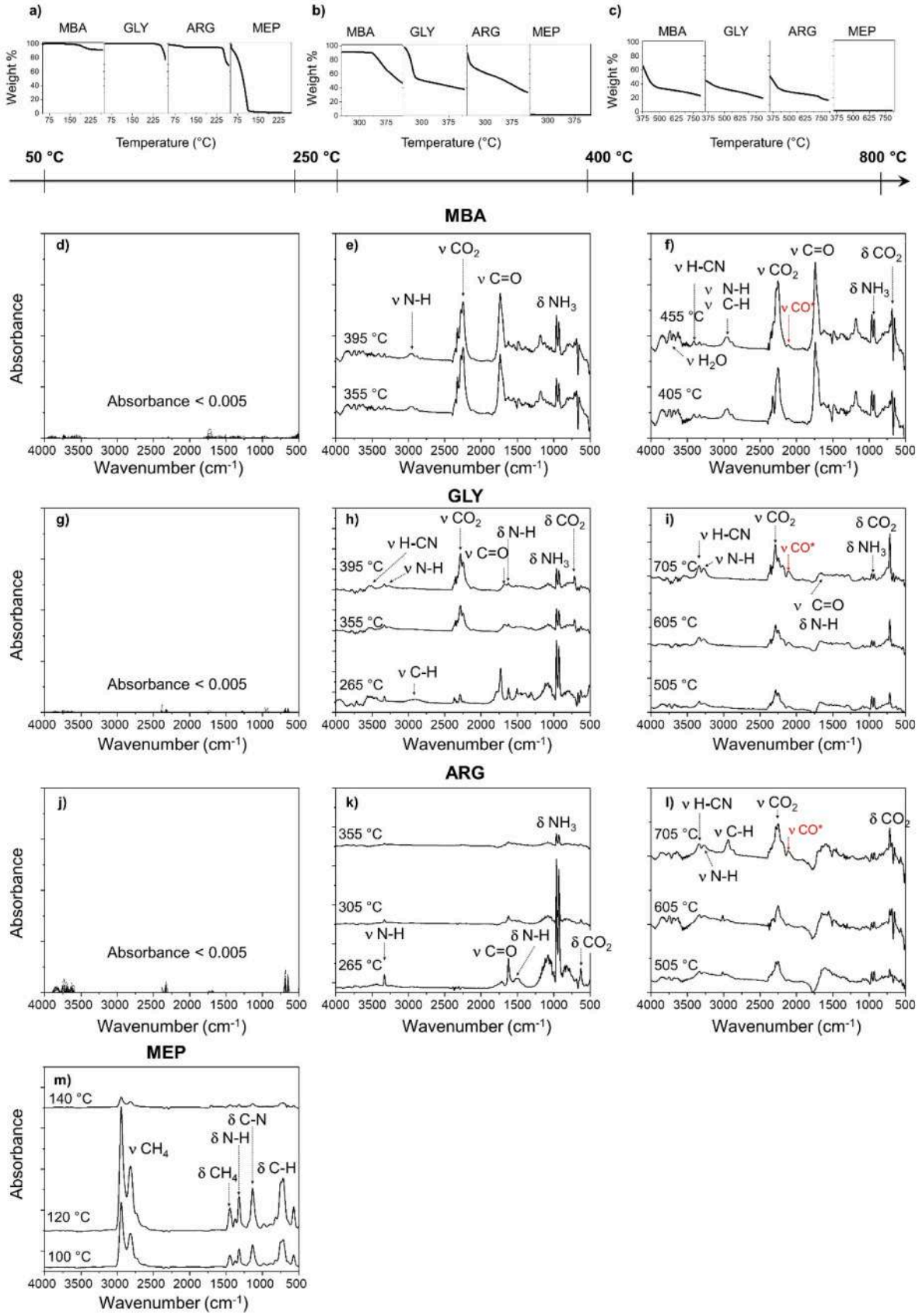

Fig. 6. TGA thermograms under inert atmosphere (nitrogen) of N,N'-methylenebisacrylamide (MBA), glycine and arginine in the temperature intervals 50–250 °C (a), 250–400 °C (b) and 400–800 °C (c). 2D plots of selected FT-IR spectra of the volatiles released under inert atmosphere (air) from MBA, glycine, arginine and 2-methylpiperazine in the temperature intervals 50–250 °C (d,g,j,m), 250–400 °C (e,h,k), 400–800 °C (f,i,l). *CO denotes that the concentration of carbon monoxide falls below the detection limit.

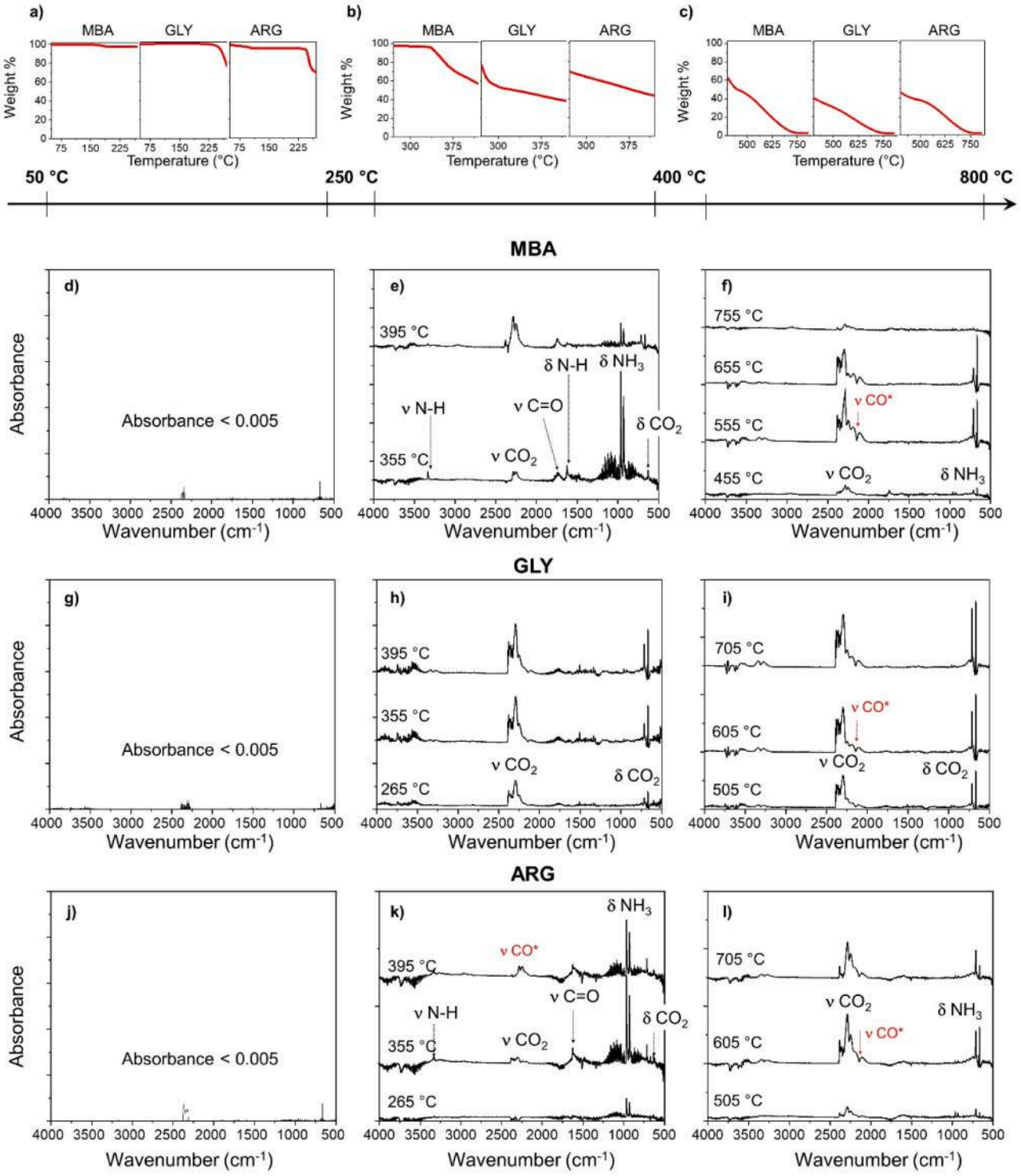

Fig. 7. TGA thermograms under oxidative atmosphere (air) of N,N'-methylenebisacrylamide (MBA), glycine and arginine in the temperature intervals 50–250 °C (a), 250–400 °C (b) and 400–800 °C (c). 2D plots of selected FT-IR spectra of the volatiles released under oxidative atmosphere (air) from MBA, glycine and arginine in the temperature intervals 50–250 °C (d,g,j), 250–400 °C (e,h,k) and 400–800 °C (f,I,l). *CO denotes that the concentration of carbon monoxide falls below the detection limit.

features in their thermal behavior (Figs. 4 and 5). For all PAAs, irrespective of temperature and atmosphere, the predominant evolved gases, although in amounts that depend on the specific temperature interval, are CO_2, NH_3 and carbonyl-containing species (hereafter referred to as "C = O"), arising from decarboxylation, deamination, cyclization and oxidation reactions (Schemes 2–6).

Hydrocarbons, arising from fragmentation of the macromolecular backbone, were observed in minor amounts from 250 °C to 800 °C.

Trace, yet significantly detectable, amounts of water were detected across the whole investigated temperature range (absorbance > 0.005), confirming the occurrence of dehydration reactions. In systems containing functional groups susceptible to intramolecular condensation, water elimination at elevated temperatures promotes cyclization, particularly the formation of thermodynamically favored five- or six-

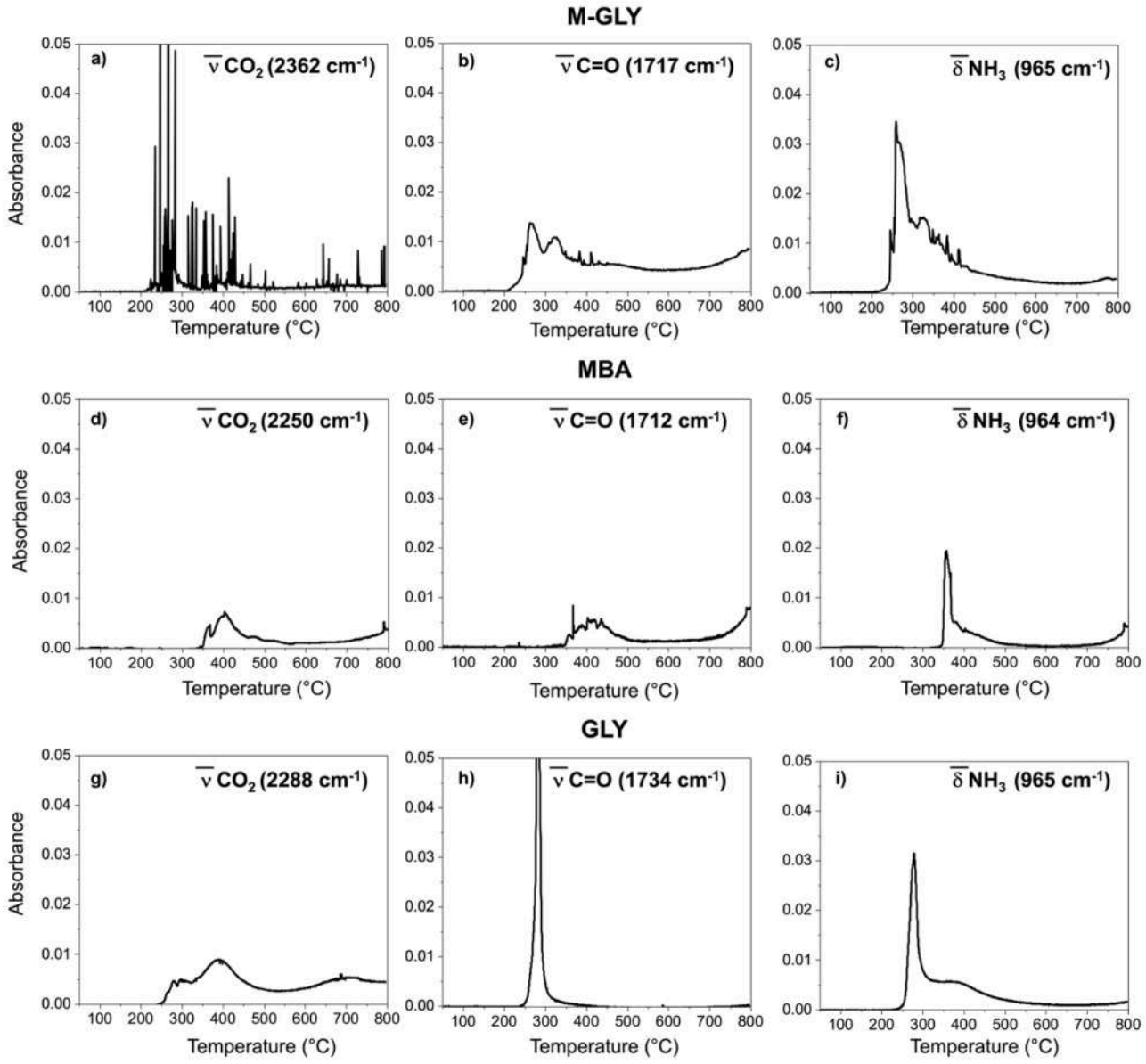

Fig. 8. Evolution profiles of the main gaseous decomposition products of M-GLY (a–c) and its monomers, MBA (d–f) and glycine (g–i), under nitrogen between 50 and 800 °C.

membered rings. These transformations increase structural rigidity and enhance conjugation within the system. Cyclodehydration often represents a preliminary step toward subsequent condensation and aromatization processes [18–20].

Notably, no evidence of nitrogen monoxide (ν (N = O), 1876 cm^{-1}) and hydrogen cyanide (HCN, ν (C—H) = 3300, ν (C≡N) = 2097 and δ (H—C≡N) 712 cm^{-1} [21]) was found the PAA spectra across the entire temperature range under both atmospheres (Table S1). Carbon monoxide (ν (C = O), centered at 2143 cm^{-1}, [22]) was also below the detection threshold. Finally, for all PAAs, a significant CO_2 release was observed in air from 400 to 800 °C, due to char oxidation.

For the sake of clarity, the gas released within the different decomposition stages discussed in Section 3.3 will be examined.

1st stage: 50–250 °C (Figs. 4 and 5, nitrogen and air). In this stage, M-GLY releases only trace amounts of gaseous decomposition products, i.e. H_2O, CO_2, NH_3, and carbonyl-containing compounds (C = O, Figs. 4d and 5d in nitrogen and air, respectively), whereas M-ARG (Figs. 4g and 5g) and M-MEP (Figs. 4j and 5j) exhibit no detectable gas release. Although in this stage the gas evolution is almost negligible, the onset of preliminary bond-cleavage events can reasonably be assumed, which precedes extensive backbone scission in the subsequent decomposition stage. A plausible mechanism is thermally induced depolymerization via a retro-aza-Michael β-elimination pathway (Scheme 2). Because the aza-Michael addition underlying PAA formation is intrinsically reversible [23,24], increasing temperature shifts the equilibrium toward bond dissociation, thereby promoting depolymerization. Mechanistically, the β-elimination process involves abstraction of the acidic proton in the α-position relative to the carbonyl group, followed by re-formation of the conjugated double bond and release of the amine. The moderate activation energies associated with retro-Michael β-elimination in β-amido amine networks (Ea ≈ 61.5 kJ mol^{-1}, onset temperature over 120–180 °C) [25], together with those reported for β-amino esters (50–80 kJ mol^{-1}) [26] and thiol-Michael adducts [27,28], suggest that depolymerization is likely initiated within this temperature window, supporting the kinetic feasibility of this mechanism. Further support for the lability of β-amino-substituted carbonyl linkages is provided by documented thermal decomposition and exchange processes involving polymeric Mannich bases in the presence of non-volatile amines [29,

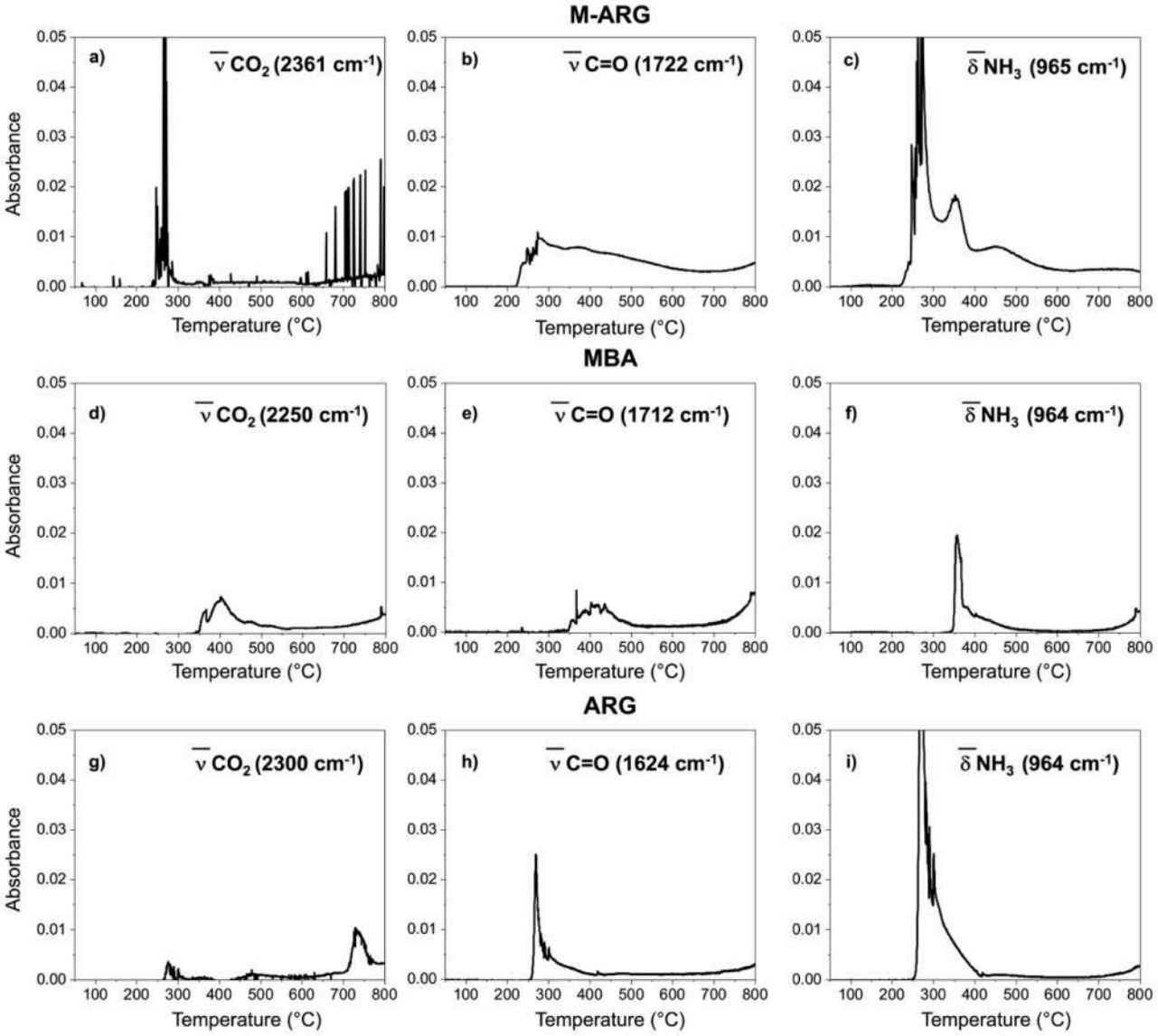

Fig. 9. Evolution profiles of the main gaseous decomposition products of M-ARG (a–c) and its monomers, MBA (d–f) and arginine (g–i), under nitrogen between 50 and 800 °C.

30].

2nd stage: 250–400 °C (Figs. 4 and 5, nitrogen and air). In this stage, PAAs exhibit an intensified evolution of CO_2, NH_3, and C = O, accompanied by the onset of hydrocarbon formation (C—H). The gaseous species released, likely originate from secondary reactions of the chain ends generated by retro-aza-Michael cleavage. Moreover, not unexpectedly, no CO_2 is released from M-MEP within this interval.

3rd stage: 400–800 °C (Figs. 4 and 5, nitrogen and air). In nitrogen, NH_3 release becomes negligible, while both M-GLY and M-ARG exhibit a markedly lower CO_2 release compared to the 2nd stage, consistent with the lower weight loss observed during the 3rd stage, whereas CO_2 release from M-MEP becomes detectable. In air, CO_2 evolution becomes significantly more pronounced, consistent with the growing kinetic contribution of oxidation reactions.

Investigating the thermal and thermo-oxidative decomposition of monomers offers valuable insight into the underlying decomposition mechanisms of PAAs, which will be discussed in section 3.4 and Schemes 2–6.

3.4. TG-FTIR analysis of monomers

A comparative analysis of the temperature-dependent gas evolution profiles of monomers provides valuable insight into the decomposition mechanisms of PAAs, particularly during the 2nd stage (250–400 °C), where the maximum mass loss occurs. The TGA thermograms and the 3D TG-FTIR spectra of MBA, glycine, arginine and 2-methylpiperazine in inert and oxidative atmospheres are shown in Fig. S4, while the 2D FT-IR spectra obtained in the different temperature intervals are shown in Fig. 6 (nitrogen) and Fig. 7 (air).

Notably, glycine and arginine exhibit significantly lower thermal stability than MBA in both atmospheres ($T_{onset} \approx 250$ °C and $T_{MAX} \approx 260$ °C for the α-amino acids vs ~350 °C and ~400 °C for MBA), reflecting fundamentally different degradation mechanisms. 2-Methylpiperazine (b.p. 155 °C, 1 atm) primarily undergoes volatilization below 200 °C (Figs. 6 and 7).

The main decomposition stage (200–320 °C) of both α-amino acids is initiated by decarboxylation via intramolecular proton transfer, generating CO_2 and zwitterionic intermediates that subsequently undergo deamination, releasing NH_3 [31–33]. These steps yield reactive imine or

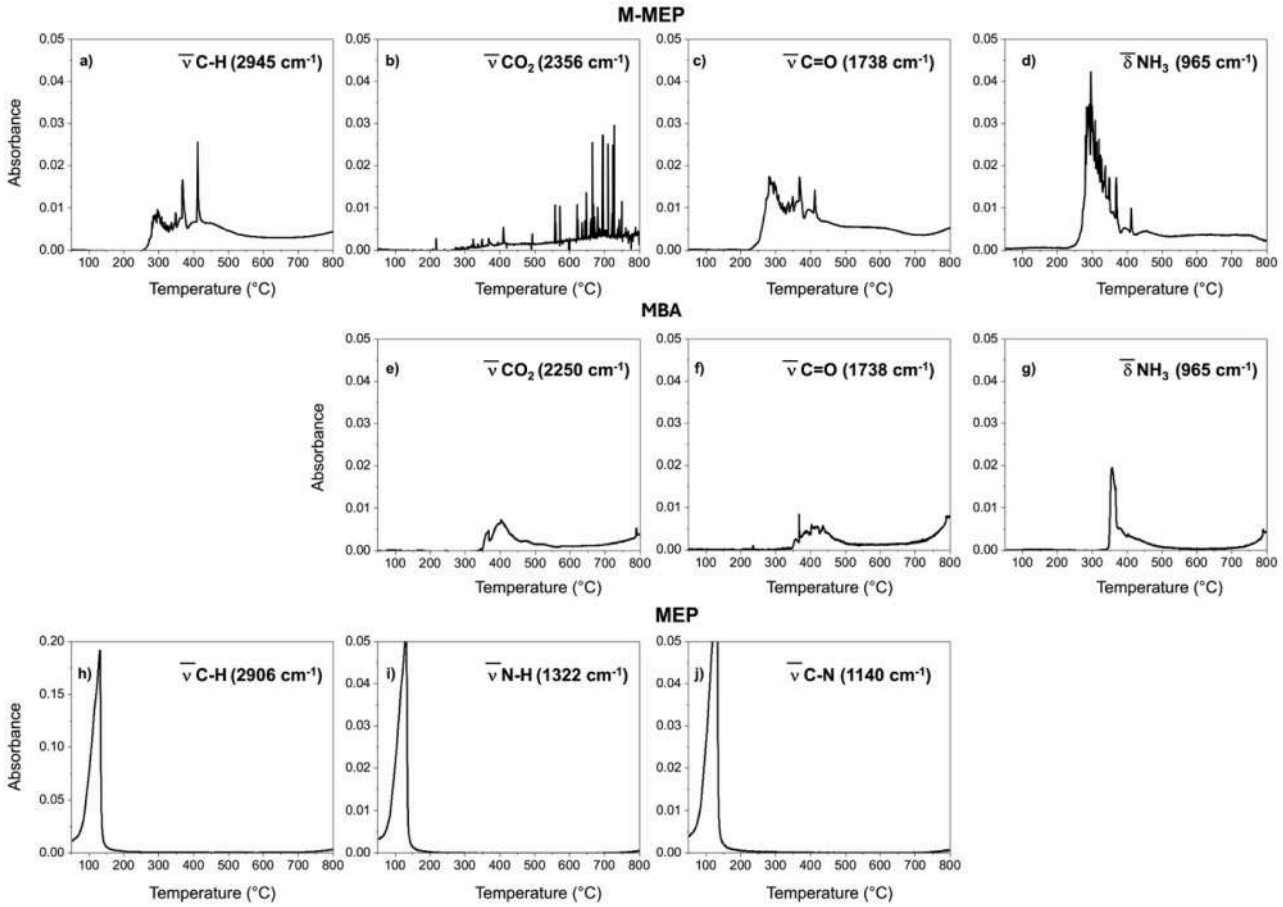

Fig. 10. Evolution profiles of the main gaseous decomposition products of M-MEP (a–d) and its monomers, MBA (e–g) and 2-methylpiperazine (h–j), under nitrogen between 50 and 800 °C.

nitrile-type species that promote secondary condensation and char formation [34]. Under inert atmosphere, CO formation at higher temperatures (>350–400 °C) arises from secondary fragmentation of carbonyl-containing intermediates and partial breakdown of the developing carbonaceous matrix (Fig. 6). Under oxidative conditions, surface and gas-phase oxidation pathways convert CO into CO_2 above 400 °C (glycine) and 450 °C (arginine), suppressing incomplete fragmentation products and enhancing total oxidation (Fig. 7).

In contrast, MBA decomposition [35] between 200 and 300 °C is triggered by homolytic C–N cleavage of the amide bond, generating nitrogen-centered and carbonyl-stabilized radicals [36]. These radicals evolve NH_3 and HCN through β-scission and rearrangement reactions, while dehydration and condensation release H_2O. Between 300 and 400 °C, fragmentation of vinyl and carbonyl groups proceeds via radical pathways, producing CO, CO_2, and small unsaturated hydrocarbons. Simultaneously, thermally induced radical polymerization of vinyl moieties promotes crosslinked network formation, which kinetically competes with volatilization and shifts extensive mass loss to higher temperatures.

3.5. *Temperature-dependent evolution of gaseous decomposition products and proposed decomposition mechanisms*

Insight into the decomposition mechanisms of PAAs can be obtained through a comparative analysis of the temperature-dependent evolution of gaseous products released from PAAs and their corresponding monomers. Figs. 8–13 report the evolution profiles of the main gaseous decomposition products of PAAs and their monomers in nitrogen (Figs. 8–10) and in air (Figs. 11–13) over the 50–800 °C range. In these figures, the profile of a single monitored band, corresponding to the most intense signal, is shown in each panel. Table S2 provides the complete list of all monitored species for the different PAAs and monomers.

Noteworthy, in both nitrogen and air, the polymer gas release curves collectively span the same temperature ranges in which these gases evolved from the corresponding monomers. These findings suggest that, within specific temperature intervals, each monomeric sub-unit contributes differently to the overall decomposition of PAAs. More specifically, following the retro-aza-Michael depolymerization step hypothesized to occur in the 1st stage (50–250 °C), the gases evolved up to approximately 350–400 °C are mainly attributable to the thermal decomposition of the amino acid (or amine) terminals. In contrast, the gaseous products released above 350–400 °C predominantly originate from the thermal degradation of the MBA-terminals. However, it is important to note here that the decomposition pathways of the two subunits are not expected to coincide exactly with those of their respective monomers, both in terms of temperature intervals and nature of the evolved gases, as the degradation of the repeating units is preceded and mediated by the depolymerization step.

The proposed decomposition patterns of PAAs under pyrolytic conditions is discussed below. For the sake of simplicity, the oxidation mechanisms have been omitted, as they are assumed to be well established.

3.5.1. *Thermal decomposition of M-GLY*

The temperature-dependent evolution of gaseous species from M-GLY (Fig. 8) reflects the distinct contributions of the two structural subunits, namely acrylamide MBA-derived terminal and the amine

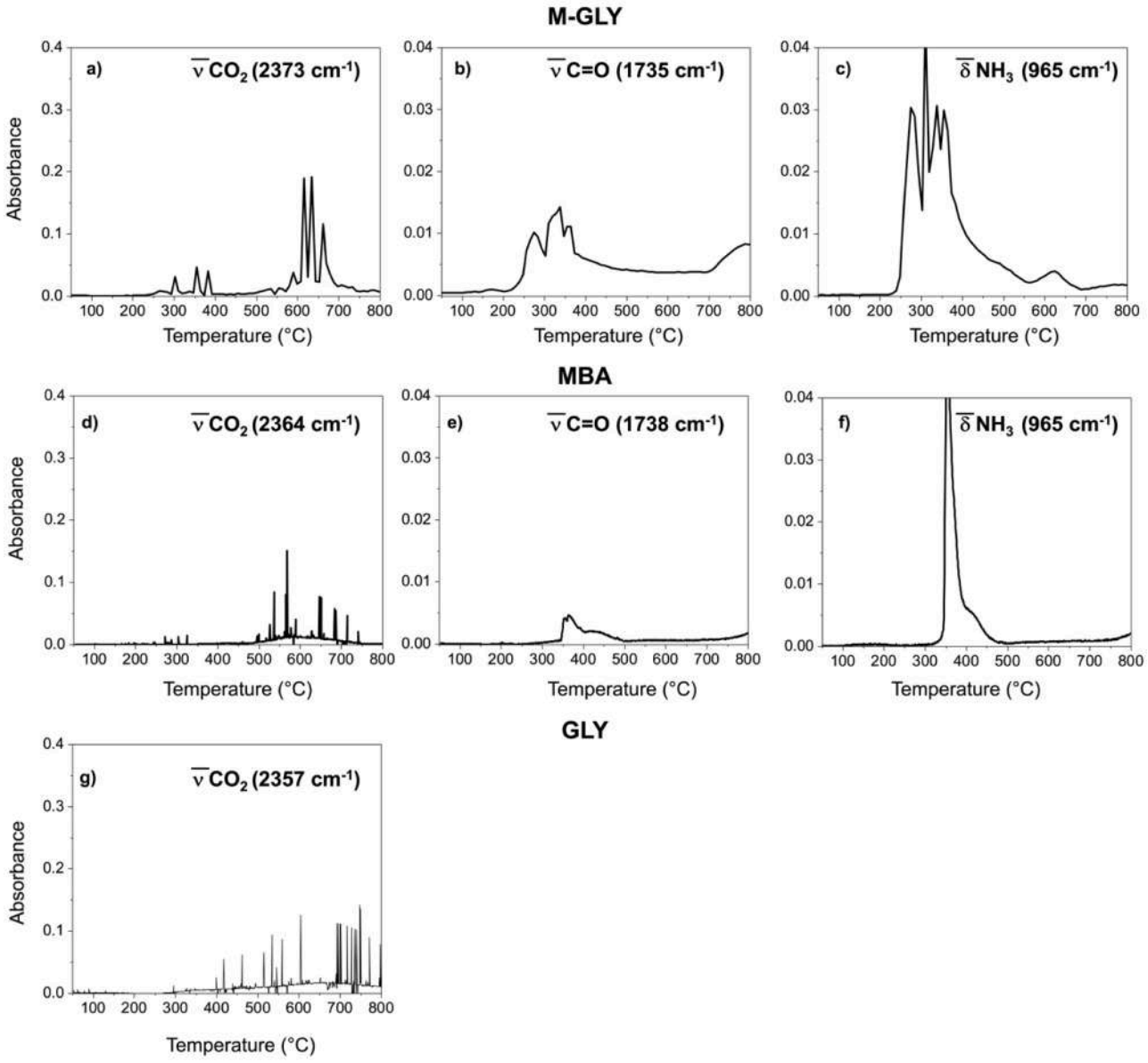

Fig. 11. Evolution profiles of the main gaseous decomposition products of M-GLY (a–c) and its monomers, MBA (d–f) and glycine (g), under air between 50 and 800 °C.

glycine-derived terminal, to the overall decomposition pathway.

Scheme 3 outlines the proposed thermal decomposition mechanism of the acrylamide chain ends originated by the retro-aza-Michael β-elimination (Scheme 2) occurring via two distinct pathways. The first pathway (Scheme 3a) involves homolytic bond cleavage, generating a macroradical chain fragment and the precursor of an acrylamide molecule that subsequently volatilizes. This agrees with the experimental observation of C = O species reported in Fig. 8b

The resulting macroradical may in turn undergo deamination reactions, leading to the evolution of CH_4 and NH_3. This is in line with the observation of significant amounts of NH_3 (Fig. 8c), while the monitored CH_4, detectable in the 3D spectra (Fig. S3), was negligible.

Alternatively, the macroradical rearrange to form aldehydes, which are likewise released as volatile decomposition products (see C = O profile in Fig. 8b). The alternative decomposition route (Scheme 3b) involves intramolecular cyclization followed by β-elimination, yielding a lactam-derived acrylamide species that may volatilize under the applied thermal conditions (see C = O profile in Fig. 8b).

Scheme 4 presents the proposed thermal decomposition mechanism of the glycine-based terminals. A first pathway (Scheme 4a) involves β-elimination, leading to the formation of glycine. However, glycine is thermally unstable at elevated temperatures and rapidly decomposes into CO_2 and NH_3 (Scheme 4b) according to the observed signal evolution in Figs. 8a and 8b, respectively.

Alternatively, glycine itself may undergo dimerization (Scheme 4d), forming species already reported in the literature and illustrated in the scheme. The detected carbonyl wavenumbers are indeed consistent with the presence of amide or lactam functionalities (Fig. 8b).

A second pathway (Scheme 4b) proceeds via decarboxylation involving the pendant carboxyl group of the repeating unit. This hypothesis is in line with the observed CO_2 evolution (Fig. 8a). Following decarboxylation, an amine-terminated species may be generated, which can further decompose with the evolution of NH_3 and CH_4 (Scheme 4f).

3.5.2. *Thermal decomposition of M-ARG*

The gas evolution profiles of M-ARG are broadly comparable to those of M-GLY, with the main difference being the greater NH_3 release observed during the 3rd decomposition stage (400–800 °C). This

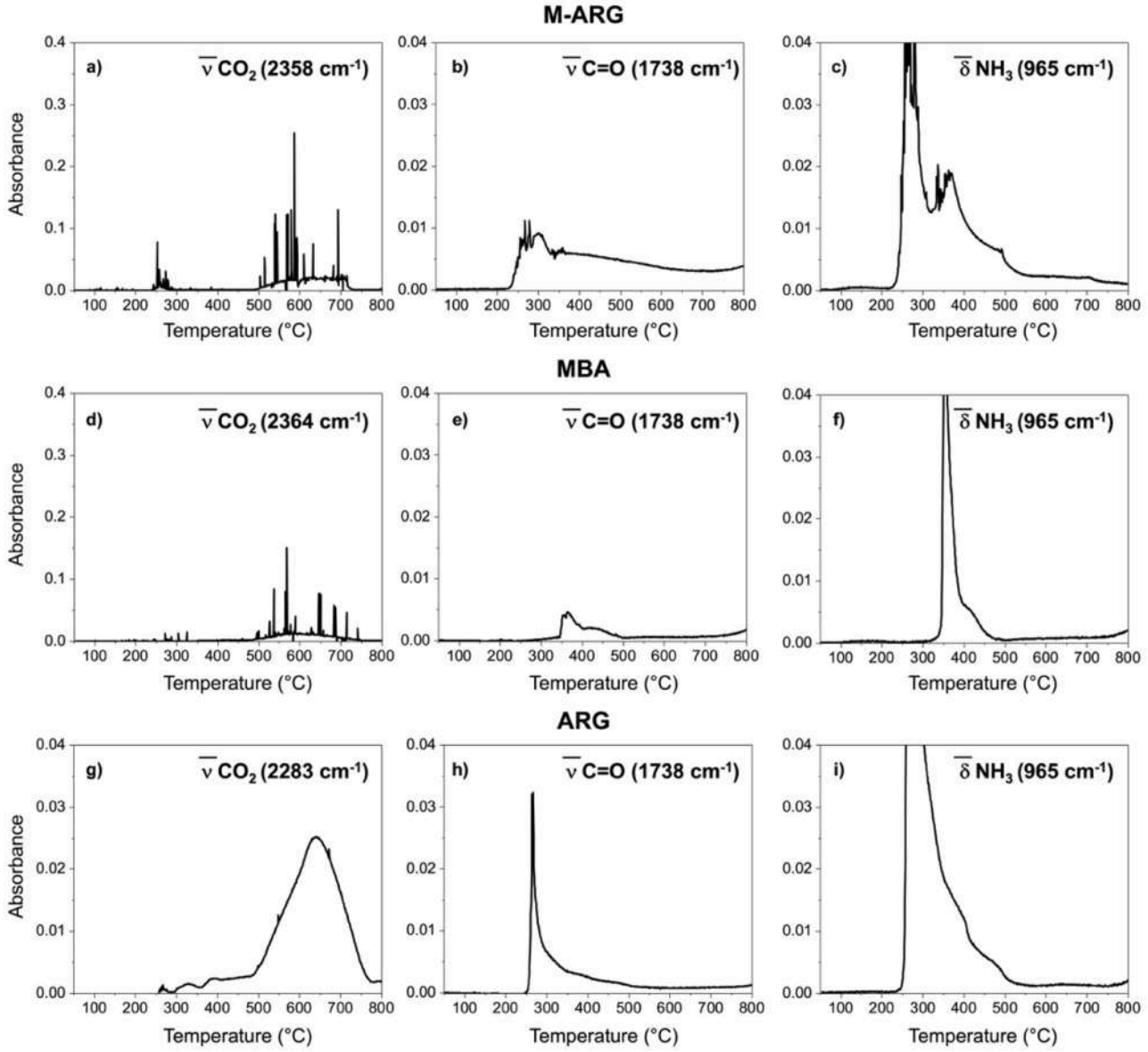

Fig. 12. Evolution profiles of the main gaseous decomposition products of M-ARG (a–c) and its monomers, MBA (d–f) and arginine (g–i), under air between 50 and 800 °C.

behavior is consistent with a negligible residue at 800 °C (RMF_{800}) measure in air for M-ARG and a 2.6% RMF_{800} for M-GLY under the same atmosphere (Table 3).

M-ARG undergoes more pronounced mass loss than M-GLY during the 1st and 2nd stages (Table 3), likely attributable to the inherent reactivity of the arginine residue, whose guanidine group readily decomposes into several gaseous products. For the arginine monomer, these gases include HCN [33]; however, it is not detected in the effluent gases of M-ARG.

Scheme 5 presents the proposed thermal decomposition mechanism of the arginine-based terminals. The decomposition is hypothesized to proceed via an initial decarboxylation step (Scheme 5a), resulting in the release of CO_2, as observed experimentally (Fig. 9a), followed by a deamination process involving the guanidinium moiety (Scheme 5b), consistent with the evolution of NH_3 (Fig. 9c). This sequence leads to the formation of a carbodiimide intermediate (Scheme 5c). A plausible mechanistic rationale for the absence of HCN among the gases evolved from M-ARG is the involvement of the highly reactive terminal carbodiimide group formed after the deamination step (Scheme 5b) into alternative reaction pathways that compete with, and potentially prevail over, HCN release. These pathways may include (i) intramolecular cyclization with adjacent functional groups and (ii) intermolecular crosslinking through reactions with neighboring macromolecular segments.

Guanidine decomposition leads to substantially greater NH_3 evolution than in M-GLY, under both nitrogen (compare Fig. 8c with Fig. 9c) and air (compare Fig. 11c with Fig. 12c) atmospheres, especially during the third stage, indicating the lower thermal stability of M-ARG char compared to that of M-GLY.

The contribution of the acrylamide terminal aligns with previous observations for M-GLY (Scheme 3). It is important to note that, in this polymer, based on the proposed mechanism, the evolution carbonyl-containing species (Fig. 9b) is not ascribed to the amine-terminals but rather to the acrylamide terminals.

3.5.3. *Thermal decomposition of M-MEP*

In the 250–350 °C range, before decomposition of the MBA-derived subunit sets in, M-MEP decomposition is primarily governed by the

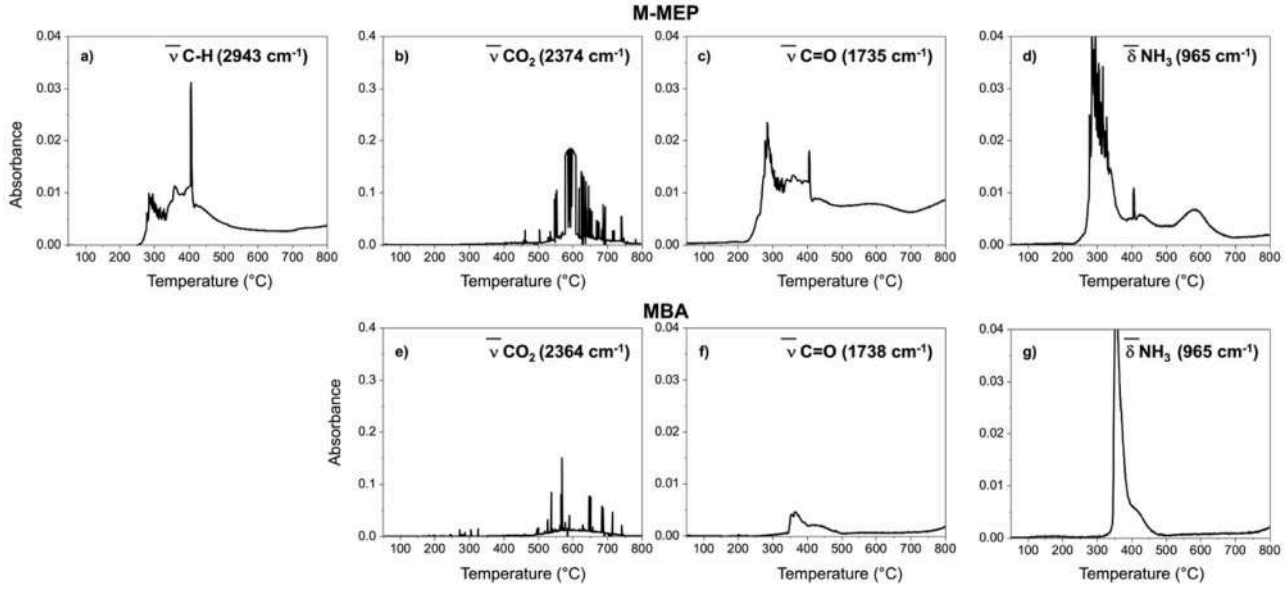

Fig. 13. Evolution profiles of the main gaseous decomposition products of M-MEP (a–d) and MBA (e–g), under air between 50 and 800 °C.

Table 2
Thermal data of M-GLY, M-ARG and M-MEP in inert and oxidative atmosphere.

Code	$T_{onset10\%}$ (°C)	T_{MAX1} (°C)		T_{MAX2} (°C)	RMF (%)	
	N_2/Air	N_2	Air	Air	N_2	Air
M-GLY	193	266	256	569	23.8	2.6
M-ARG	226	221	241/277/349	525	17.9	0.0
M-MEP	213	221	267/363	559	14.4	0.0

Table 3
Weight loss of data of M-GLY, M-ARG and M-MEP in inert and oxidative atmosphere.

Code	Weight loss (%)				
	1st stage 50–250 °C	2nd stage 250–400 °C		3rd stage 400–800 °C	
	N_2/Air	N_2	Air	N_2	Air
M-GLY	22.1	40.6	36.5	13.5	38.8
M-ARG	21.8	42.2	37.2	18.1	41.0
M-MEP	14.2	53.0	51.6	18.0	34.2

volatility of 2-methylpiperazine, accounting for the early detection of C–H fragments and NH_3 (from 250 °C) (Figs. 10a and 10d, respectively).

The pronounced thermal lability of M-MEP explains why it undergoes the highest weight loss among all PAAs in both nitrogen and air during the 1st and 2nd stages (Table 3).

The proposed thermal decomposition pathway of the 2-methylpiperazine terminals appears comparatively straightforward (Scheme 6). The initial step involves the evolution of the 2-methylpiperazine monomer (boiling point ≈ 155 °C at 1 atm), accompanied by the formation of a vinyl-terminated chain fragment (Scheme 6a).

The release of 2-methylpiperazine has important implications for the fire behavior of M-MEP. Unlike M-GLY and M-ARG, which do not sustain combustion under direct flame impingement and instead form a stable protective char layer that shields the underlying material, M-MEP is flammable and burns under the same conditions [10]. This difference can be rationalized by considering that 2-methylpiperazine is classified as flammable [37,38] and is known to generate combustible species upon heating [39]. Therefore, its evolution during thermal decomposition likely contributes to sustained combustion in M-MEP, while simultaneously limiting the formation of a protective char. Following its release, 2-methylpiperazine may undergo further transformations, in analogy with decomposition pathways reported for piperazine [40,41].

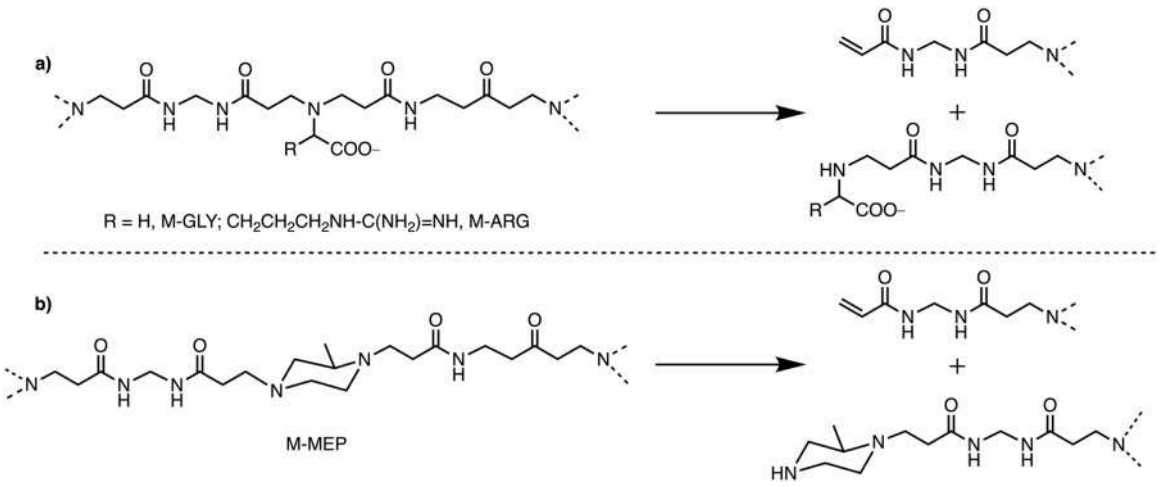

Scheme 2. Retro-aza-Michael depolymerization reaction of PAAs.

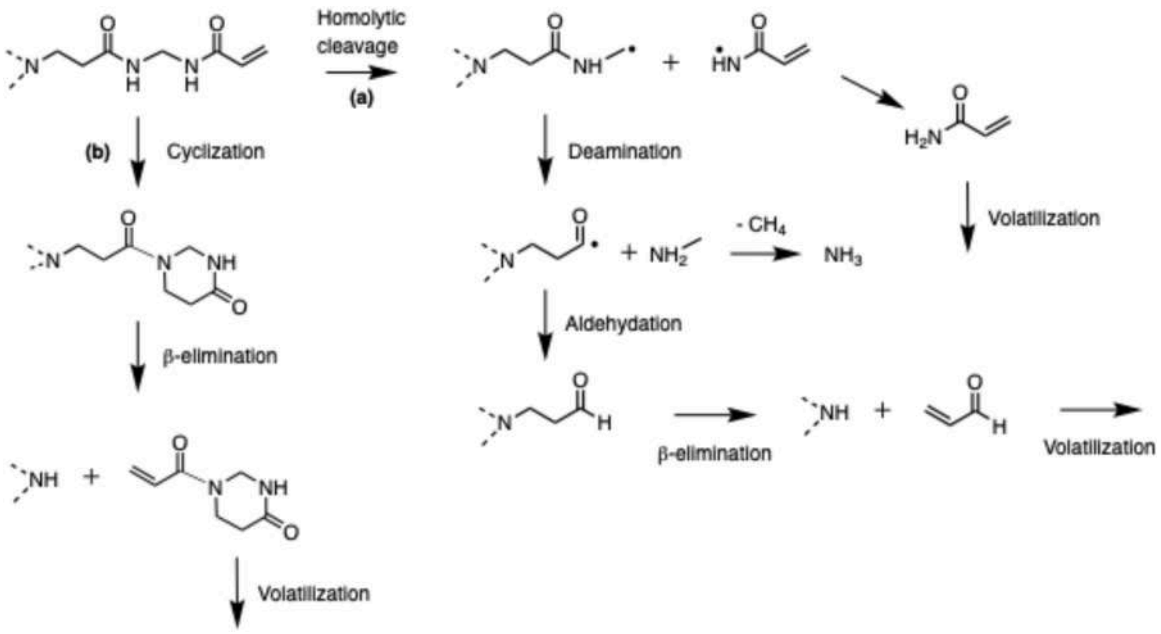

Scheme 3. Proposed mechanism of thermal decomposition of acrylamide terminals.

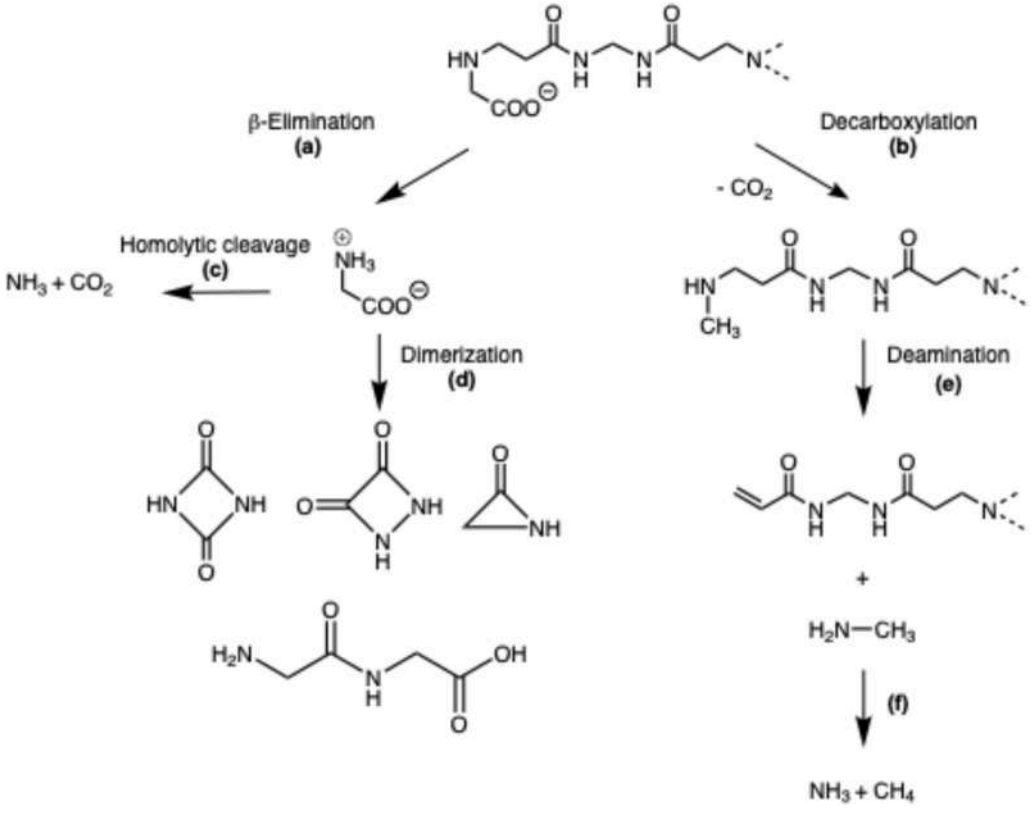

Scheme 4. Proposed mechanism of thermal decomposition of the glycine-based terminals.

These secondary processes ultimately lead to the formation of ammonia and low-molecular-weight hydrocarbon species as volatile products.

The contribution of the acrylamide terminal aligns with previous observations for M-GLY (Scheme 3). It is important to note that, in this polymer, according to the proposed mechanism, the formation of carbonyl-containing species (Fig. 9b) is attributed not to the amine terminals, but rather to the acrylamide terminals.

4. Conclusions

The combined use of thermogravimetric analysis and FT-IR spectroscopy of the evolved gases, collected during heating from 50 to 800 °C under inert and oxidative atmospheres, provided detailed insight into the thermal and thermo-oxidative degradation behavior of three MBA-derived PAAs, namely M-GLY, M-ARG and M-MEP, obtained from the reaction of MBA with the α-amino acids glycine and arginine and with 2-

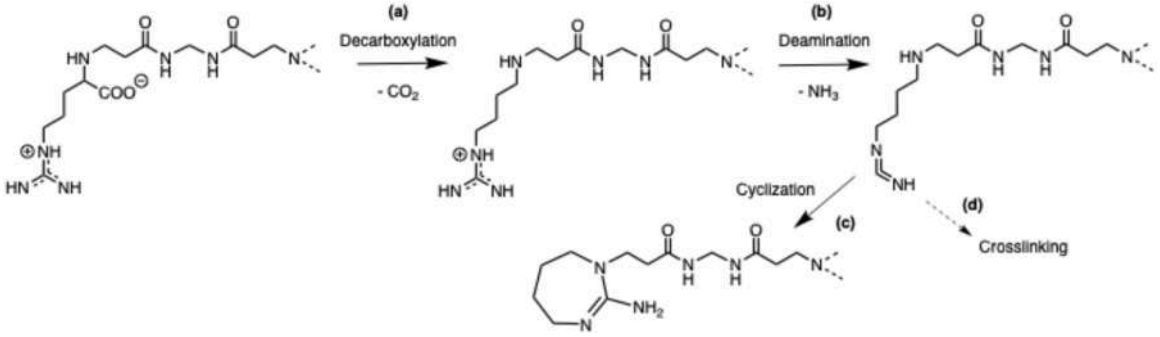

Scheme 5. Proposed mechanism of thermal decomposition of the arginine-based terminals.

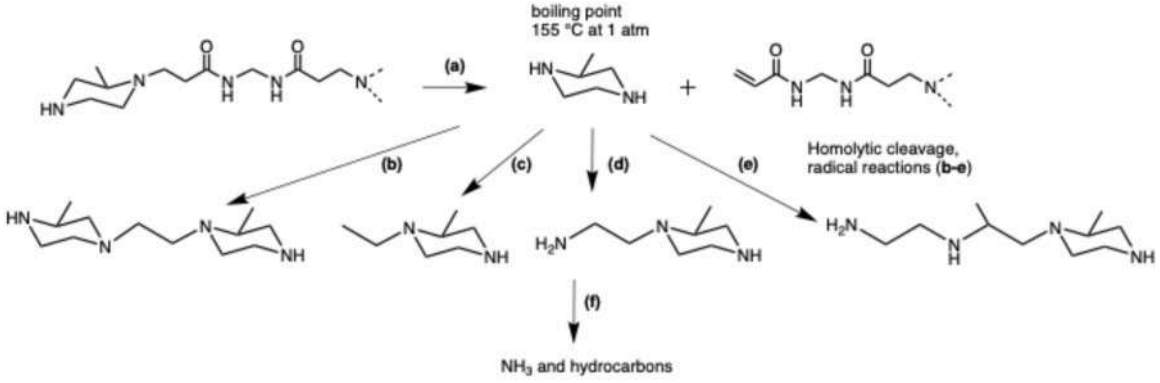

Scheme 6. Proposed mechanism of thermal decomposition of the 2-methylpiperazine-based terminals.

methylpiperazine, respectively.

The identification of their gaseous decomposition products within well-defined temperature intervals not only elucidated their decomposition pathways but also clarified their gas-phase mode of action as flame retardant coatings for cotton, explaining their effectiveness.

The analysis of the TGA thermograms indicates that oxidative reactions become kinetically significant above 400 °C, where they begin to compete with purely pyrolytic pathways and predominantly yield combustion gases. Since the main mass loss occurs between 250 and 400 °C, the mechanistic investigation primarily focuses on the processes taking place within this temperature range.

The fundamental hypothesis was that the above PAAs start decomposing below 200 °C through distinct mechanisms, namely a retro-aza-Michael depolymerization reaction and a C—N homolytic dissociation involving the central methylene group of the MBA-derived moiety. The homolytic cleavage involving the bisacrylamide-derived moiety implies the same structural evolution for all three PAAs, and includes a series of cyclization, deamination and β-elimination reactions, significantly contributing to NH_3 evolution.

Depolymerization regenerates the original amine and bisacrylamide end groups and, if it proceeds, may lead to the release of amines. When the amine is relatively volatile, as in the case of 2-methylpiperazine, a recognized flammable compound known to generate combustible species upon heating, it is rapidly removed from the equilibrium during the early heating stages (around 150 °C), migrates to the gas phase and, under combustion conditions, may ignite and burn, thereby compromising any potential protective effect. Conversely, when the amine monomer is an α-amino acid, it undergoes different reaction pathways upon heating, such as cyclization, decarboxylation, or deamination, generating gaseous species, such as ammonia and carbon dioxide, which dilute oxygen and flame radicals and induce cooling through endothermic decomposition and volatilization.

Similarly, the acrylamide terminals can undergo radical-induced thermal polymerization, thereby promoting the formation of aliphatic char residues. These residues are stable under an inert atmosphere ($RMF_{400} \geq 30\%$ for all three PAAs) and exhibit even greater stability under oxidative conditions due to intumescence, undergoing significant degradation only above 550 °C. The subsequent decomposition of the char releases non-flammable species, primarily ammonia and carbon dioxide.

Overall, M-GLY and M-ARG show qualitatively similar gas evolution profiles, although M-ARG releases greater amounts of ammonia during the 3rd heating stage compared with M-GLY. This observation reflects the fact that M-GLY exhibits an RMF_{800} of 2–3%, to be compared with an undetectable RMF_{800} in the case of M-ARG, and suggests a greater char stability of M-GLY with respect to M-ARG:

The proposed decomposition mechanisms suggest that the pronounced gas-phase flame-retardant action of α-amino acid-based PAAs is associated with the release, upon heating, of significant amounts of CO_2 and NH_3, which dilute oxygen and thereby mitigate oxidative processes. From a broader perspective, these findings will be further strengthened by combining them with studies on the structural evolution of PAA-derived chars under thermo-oxidative conditions, enabling deeper insight into their condensed-phase mechanism of action as flame retardants for cotton.

CRediT authorship contribution statement

Jenny Alongi: Writing – review & editing, Supervision, Conceptualization. **Alessandro Beduini:** Methodology, Investigation. **Elisabetta Ranucci:** Writing – original draft, Supervision, Funding acquisition, Conceptualization.

Declaration of competing interest

The authors declare that they have no known competing financial

interests or personal relationships that could have appeared to influence the work reported in this paper.

Acknowledgments

The Authors thank the Italian Ministry for the University and Research, project PRIN2022 N° 202237JYZN, for financial support.

Supplementary materials

Supplementary material associated with this article can be found, in the online version, at doi:10.1016/j.polymdegradstab.2026.112212.

Data availability

The data that has been used is confidential.

References

[1] E. Ranucci, A. Manfredi, Polyamidoamines: versatile bioactive polymers with potential for biotechnological applications, Chem. Afr. 2 (2019) 167–193, https://doi.org/10.1007/s42250-019-00046-1.
[2] L. Mascheroni, V. Francia, B. Rossotti, E. Ranucci, P. Ferruti, D. Maggioni, A. P. Salvati, Light-triggered trafficking to the cell nucleus of a cationic polyamidoamine functionalized with ruthenium complexes, ACS Appl. Mater. Interfaces 12 (2020) 34576–34587, https://doi.org/10.1021/acsami.0c08033.
[3] R. Duncan, P. Ferruti, D. Sgouras, A. Tuboku-Metzger, E. Ranucci, F. Bignotti, A polymer-triton x-100 conjugate capable of PH-dependent red blood cell lysis: a model system illustrating the possibility of drug delivery within acidic intracellular compartments, J. Drug Target. 2 (1994) 341–347, https://doi.org/10.3109/10611869409015915.
[4] E. Ferrari, E. Ranucci, U. Edlund, A.-C. Albertsson, Design of renewable poly (amidoamine)/hemicellulose hydrogels for heavy metal adsorption, J. Appl. Polym. Sci. 132 (2015) 41695, https://doi.org/10.1002/app.41695.
[5] S. Treccani, J. Alongi, P. Ferruti, E. Ranucci, α-amino acid-derived polyamidoamines as photostabilizers for cotton, Polym. Degrad. Stabil 239 (2025) 111430, https://doi.org/10.1016/j.polymdegradstab.2025.111430.
[6] L. Sartore, M. Penco, S. Della Sciucca, G. Borsarini, V. Ferrari, New carbon black composite vapor detectors based on multifunctional polymers, Sensors Actuat. B Chem. 111-112 (2005) 160–165, https://doi.org/10.1016/j.snb.2005.07.032.
[7] J. Alongi, E. Ranucci, Flame retardant applications of polyamidoamine dendrimers (PAMAM) and linear polyamidoamines (PAAs) in plastics and textiles, Polym. Degrad. Stabil. 241 (2025) 111516, https://doi.org/10.1016/j.polymdegradstab.2025.111516.
[8] C. Forte, J. Alongi, A. Beduini, S. Borsacchi, L. Calucci, F. Carosio, P. Ferruti, E. Ranucci, The thermo-oxidative behavior of cotton coated with an intumescent flame retardant glycine-derived polyamidoamine: a multi-technique study, Polymers (Basel) 13 (2021) 4382, https://doi.org/10.3390/polym13244382.
[9] M. Pierigé, M. Arioli, J. Alongi, E. Ranucci, C. Forte, S. Pizzanelli, Exploring the flame retardant mechanism of α-amino acid-derived polyamidoamine-treated cotton: an EPR study, Colloids Surf. A Physicochem. Eng. Asp. 728 (2026) 138787, https://doi.org/10.1016/j.colsurfa.2025.138787.
[10] A. Manfredi, F. Carosio, P. Ferruti, E. Ranucci, J. Alongi, Linear polyamidoamines as novel biocompatible phosphorus-free surface-confined intumescent flame retardants for cotton fabrics, Polym. Degrad. Stabil. 151 (2018) 52–64, https://doi.org/10.1016/j.polymdegradstab.2018.02.020.
[11] A. Beduini, F. Carosio, P. Ferruti, E. Ranucci, J. Alongi, Sulfur-based copolymeric polyamidoamines as efficient flame-retardants for cotton, Polymers (Basel) 11 (2019) 1904, https://doi.org/10.3390/polym11111904.
[12] E. Ranucci, J. Alongi, Thermal decomposition of cellulosic materials: insights into mechanisms and product evolution, Polym. Degrad. Stabil. 242 (2025) 111629, https://doi.org/10.1016/j.polymdegradstab.2025.111629.
[13] J.O. Lephardt, Fourier transform infrared evolved gas analysis (FT-IR-EGA) - another pyrolytic tool. Analytical Pyrolysis Techniques and Applications, 1984, pp. 95–120, https://doi.org/10.1016/B978-0-408-01417-5.50008-1.
[14] N. Fedelich, TGA-FTIR. Evolved Gas Analysis, Hanser Publishers, Munich; Hanser Publications, Cincinnati, USA, 2019, pp. 18–30. Chapter 3.
[15] D.A. Tomalia, H. Baker, J. Dewald, M. Hall, G. Kallos, S. Martin, J. Roeck, J. Ryder, P. Smith, A new class of polymers: starburst-dendritic macromolecules, Polym. J. 17 (1985) 117–132, https://doi.org/10.1295/polymj.17.117.
[16] J.D. Peterson, S. Vyazovkin, C.A. Wight, Kinetics of the thermal and thermo-oxidative degradation of polystyrene, polyethylene and poly(propylene), Macromol. Chem. Phys. 202 (2001) 775–784, 1022-1352/2001/0603–0775$17.50 +.50/0TG.
[17] P.J. Linstrom, W.G. Mallard (Eds.), NIST Chemistry WebBook, NIST Standard Reference Database 69, National Institute of Standards and Technology, Gaithersburg, MD, 2017.
[18] D. Jiang, J. Li, S. Wang, H. Li, L. Qian, B. Li, H. Cheng, Y. Hu, X. Hu, Cyclic compound formation mechanisms during pyrolysis of typical aliphatic acidic amino acids, ACS Sustain. Chem. Engin. 8 (2020) 16968–16978, https://doi.org/10.1021/acssuschemeng.0c07108.
[19] J.A. Joule, K. Mills, Heterocyclic Chemistry, 5th ed.; Wiley, 2010.
[20] H.G. Shaaban, F.W. Askar, A review on benzimidazoles: synthesis, properties, and therapeutic applications in medicinal chemistry, Appl. Chem. Engin. 8 (2025) 1–29, https://doi.org/10.59429/ace.v8i2.5647.
[21] S. Ghanekar, G.P. Horn, R.M. Kesler, R. Rajasegar, J. Yoo, T. Lee, Quantification of elevated hydrogen cyanide (HCN) concentration typical in a residential fire environment using mid-IR tunable diode laser, Appl. Spectrosc. 77 (2023) 382–392, https://doi.org/10.1177/00037028231152498.
[22] L. Zamirri, S. Casassa, A. Rimola, M. Segado-Centellas, C. Ceccarelli, P. Ugliengo, IR spectral fingerprint of carbon monoxide in interstellar water ice models, Mon. Not. R. Astron. Soc. 480 (2018) 1427–1444, https://doi.org/10.1093/mnras/sty1927.
[23] C. Wiles, P. Watts, "Micro Reaction Technology in Organic Synthesis", CRC Press, Boca Raton, USA, 2011. Chapter 3.3.7.
[24] R. Baruah, A. Kumar, R.R. Ujjwal, S. Kedia, A. Ranjan, U. Ojha, Recyclable thermosets based on dynamic amidation and Aza-Michael addition chemistry, Macromolecules 49 (2016) 7814–7824, https://doi.org/10.1021/acs.macromol.6b01807.
[25] L.T. Nguyen, A. Tharayil, N. Badi, J.M. Winne, F.E. Du Prez, Exploring transamidation and chemical recycling of β-amino amide-derived covalent adaptable networks, Polym. Chem. 16 (2025) 5009–5018, https://doi.org/10.1039/d5py00959f.
[26] C. Taplan, M. Guerre, F.E. Du Prez, Covalent, adaptable networks using β-amino esters as thermally reversible building blocks, J. Am. Chem. Soc. 143 (2021) 9140–9150, https://doi.org/10.1021/jacs.1c03316.
[27] C.J. Stubbs, A.L. Khalfa, V. Chiaradia, J.C. Worch, A.P. Dove, Intrinsically re-curable photopolymers containing dynamic thiol-Michael Bonds, J. Am. Chem. Soc. 144 (2022) 11729–11735, https://doi.org/10.1021/jacs.2c03525.
[28] B. Zhang, P. Chakma, M.P. Shulman, J. Ke, Z.A. Digby, D. Konkolewicz, Probing the mechanism of thermally driven thiol-Michael dynamic covalent chemistry, Org. Biomol. Chem. 16 (2018) 2725–2734, https://doi.org/10.1039/C8OB00397A.
[29] A.S. Angeloni, P. Ferruti, M. Tramontini, M. Casolaro, The Mannich bases in polymer synthesis: 3. Reduction of poly(β-aminoketone)s to poly(γ-aminoalcohol)s and their N-alkylation to poly(γ-hydroxy quaternary ammonium salt)s, Polymer (Guildf) 23 (1982) 1693–1697, https://doi.org/10.1016/0032-3861(82)90197-5.
[30] N. Ghedini, C. Della Casa, P. Costa Bizzarri, P. Ferruti, The Mannich bases in polymer synthesis, 8. Synthesis of poly[(alkylimino)alkylene(alkylimino) methylene-(2-hydroxy-5-methyl-1,3-phenylene)methylene]s, Makromol. Chem. Rapid Commun. 5 (1984) 181–186, https://doi.org/10.1002/marc.1984.030050312.
[31] Z. Wang, J. Shen, X. Liu, S. Wang, S. Deng, Z. Han, H. Zhang, Y. Guo, In-depth understanding the pyrolysis behavior of arginine: combined experiments, ReaxFF molecular dynamics and DFT calculation study, Fuel 381 (2025) 133401, https://doi.org/10.1016/j.fuel.2024.133401.
[32] J. Li, Z. Wang, X. Yang, L. Hu, Y. Liu, C. Wang, Evaluate the pyrolysis pathway of glycine and glycylglycine by TG–FTIR, J. Anal. Appl. Pyrolysis 80 (2007) 247–253, https://doi.org/10.1016/j.jaap.2007.03.001.
[33] L. Leng, L. Yang, H. Zu, J. Yang, Z. Ai, W. Zhang, H. Peng, H. Zhan, H. Li, Q. Zhong, Insights into glycine pyrolysis mechanisms: integrated experimental and molecular dynamics/DFT simulation studies, Fuel 351 (2023) 128949, https://doi.org/10.1016/j.fuel.2023.128949.
[34] I.M. Weiss, C. Muth, R. Drumm, H.O.K. Kirchner, Thermal decomposition of the amino acids glycine, cysteine, aspartic acid, asparagine, glutamic acid, glutamine, arginine and histidine, BMC Biophys. 11 (2018) 2, https://doi.org/10.1186/s13628-018-0042-4.
[35] A. Avşar, Y. Gökbulut, B. Ay, S. Serin, A novel catalyst system for the synthesis of N,N′-methylenebisacrylamide from acrylamide, Des. Monomers Polym. 20 (2017) 434–440, https://doi.org/10.1080/15685551.2017.1332138.
[36] C.D. Vlad, M.V. Dinu, S. Drăgan, Thermogravimetric analysis of some crosslinked acrylamide copolymers and ion exchangers, Polym. Degrad. Stabil. 79 (2003) 153–159, https://doi.org/10.1016/S0141-3910(02)00268-9.
[37] Sigma-Aldrich (Merck KGaA), Safety Data Sheet: 2-Methylpiperazine, Darmstadt, Germany, 2023.
[38] Thermo Fisher Scientific. Safety Data Sheet: 2-Methylpiperazine, Waltham, MA, USA, 2025.
[39] National Center for Biotechnology Information, PubChem Compd. Summ. 2-Methylpiperazine, https://pubchem.ncbi.nlm.nih.gov.
[40] S.A. Mazari, B. Si Ali, B.M. Jan, I.M. Saeed, Degradation study of piperazine, its blends and structural analogs for CO_2 capture: a review, Int. J. Greenh. Gas Control 31 (2014) 214–228, https://doi.org/10.1016/j.ijggc.2014.10.003.
[41] S.A. Freeman, G.T. Rochelle, Thermal degradation of aqueous piperazine for CO_2 capture: 2. Product types and generation rates, Ind. Eng. Chem. Res. 51 (2012) 7726–7735, https://doi.org/10.1021/ie201917c.